Resonant coupling effects on the photoassociation of ultracold Rb and Cs atoms

B. E. Londoño,[1,2] J. E. Mahecha,[1] E. Luc-Koenig,[2,*] and A. Crubellier[2]
[1]*Instituto de Física, Universidad de Antioquia, Calle 67 No 53-108, AA 1226 Medellin, Colombia*
[2]*Laboratoire Aimé Cotton, CNRS, Université Paris-Sud 11, Bâtiment 505, 91405 Orsay Cedex, France*
(Received 29 April 2009; revised manuscript received 27 July 2009; published 14 September 2009)

In the polar RbCs molecule, the strong spin-orbit coupling between the $A\,^1\Sigma^+$ and $b\,^3\Pi$ diabatic electronic states correlated to the Rb($5s$)Cs($6p$) dissociation limit is at the origin of a global mixing of the two vibrational $0^+(P_{1/2,3/2})$ series coupled radiatively to both $X\,^1\Sigma^+$ and $a\,^3\Sigma^+$ states. This so-called "resonant coupling" plays a crucial role in the formation of ultracold stable RbCs molecules through photoassociation into 0^+ levels followed by stabilization through spontaneous emission. We analyze quantitatively the mechanisms of photoassociation and stabilization through 0^+ levels, starting from and leading to either the singlet or the triplet states and we compare the efficiency of the four paths leading to the formation of stable RbCs molecules. Comparison between the two isotopomers ^{87}Rb^{133}Cs and ^{85}Rb^{133}Cs is also reported: the overall process of formation of stable molecules is one order of magnitude larger for ^{87}RbCs. The simple two-channel model presented here yields the general rules for a standard analysis of the effects of resonant coupling between electronic states. To underline the specificity of heteronuclear molecules, the 0^+ coupled system of the RbCs molecule is compared to its analog, the 0_u^+ system of the Rb_2 molecule.

DOI: 10.1103/PhysRevA.80.032511 PACS number(s): 33.20.−t, 37.10.Mn, 37.10.Pq, 82.50.Nd

I. INTRODUCTION

In recent years, in view of both their internal properties and their mutual interactions, there has been a great interest in producing dense samples of heteronuclear molecules at ultralow temperature ($T<1$ mK) (for a recent review of ultracold dipolar molecules see [1,2] and references therein). In particular, heteronuclear alkali-metal dimer molecules can possess a large permanent electric dipole moment [3], which offers unique possibilities for fundamental physics experiments, such as the search for a permanent dipole moment of the electron or parity violation [4,5]. Furthermore, in these systems, the existence of nearly degenerate pairs of vibrational levels associated with different electronic potentials renders possible high resolution studies for testing the variations of fundamental constants [6–8]. The long-range interaction between two polar molecules is governed by the anisotropic electric dipole-dipole interaction, which gives rise to many unique phenomena typical of highly correlated quantum many-body states, which are observable in Bose-Einstein condensates [9] or in molecules trapped in optical lattices. There are also possibilities for quantum computation [10–12], for cold chemistry [13,14] or for the realization and the control of different phase transitions, including superfluid, supersolid, and Mott insulating phases [15–19], for example.

Many of these experiments require dense and ultracold samples of molecules in a deep well-defined rovibrational level of either the stable ground electronic state $X\,^1\Sigma_{(g)}^+$ (X) or the metastable lowest triplet state $a\,^3\Sigma_{(u)}^+$ (a) (the "gerade" g and "ungerade" u symbols label symmetry under the exchange of nuclear centers and apply only to homonuclear species). In fact, samples of molecules in the "absolute ground level," i.e., the $X\,^1\Sigma_{(g)}^+$ level with vibrational $v''=0$ and rotational $J''=0$ quantum numbers, are the most desirable. Such samples cannot readily be obtained by direct cooling of ground-state molecules through buffer gas cooling [20] or Stark deceleration [21] methods, for example. In contrast, neutral alkali-metal atoms can be trapped and laser cooled at ultracold temperature (80–100 μK) and, to date, the coldest and highest-density samples of stable alkali-metal dimers in the X or a state have been created by the association of ultracold atoms via magnetic-field Feshbach resonances [22], photoassociation in an excited electronic state followed by stabilization through spontaneous emission [23] or, more recently, radiofrequency magnetic-dipole transitions [24,25].

However, these molecules are generally not formed in the lowest lying level $v''=0$, $J''=0$ of the ground electronic state but in highly excited levels of either the X or the a state. Processes for transferring these excited stable molecules toward lower lying levels have been investigated. In homonuclear molecules, due to the $g\leftrightarrow u$ selection rule for electric dipole transitions, a two-step optical excitation-deexcitation process permits only a vibrational cooling [26,27] (for molecules created in an incoherent superposition of vibrational levels) or a coherent transfer (for molecules created in a single level), such as stimulated Raman adiabatic passage (STIRAP) [28,29] within the X or the a electronic state. For heteronuclear species, a two-step "conversion process" from the a state toward the X state is allowed through excitation of intermediate levels with a mixed singlet-triplet spin character. Such conversion processes have been recently investigated theoretically [30,31] and experimentally [32,33].

Ultracold stable polar molecules in their vibronic ground level have been produced for the first time by Sage *et al.* for the RbCs molecule using a four photon process (photoassociation and radiative decay followed by a two-color incoherent transfer) [32]. Recently Deiglmayr *et al.* [34,35] directly obtained ultracold ^{7}Li^{133}Cs molecules in the absolute ground level via a single photoassociation step at large laser detun-

*eliane.luc@lac.u-psud.fr

ing followed by spontaneous emission. Using a STIRAP process, Ni *et al.* [33] transferred extremely weakly bound stable $^{40}K^{87}Rb$ molecules, obtained through Feshbach resonance in the a electronic state, toward the lowest vibrational level of either the stable X state or the metastable a state.

An efficient scheme for the obtention of cold molecules consists of starting from cold and dense atomic samples to form molecules by photoassociation (PA) of atom pairs. Spontaneous radiative stabilization (RS) of the short-lived photoassociated molecules leads then to cold stable molecules. However, the photoassociated molecule generally decays through transition at large internuclear distance, populating mainly continuum levels, i.e., giving back pairs of hot atoms and eventually molecules in a few of the uppermost bound levels of the ground electronic state. When stabilization occurs at shorter distance, especially close to the inner wall of the excited potential, deeper bound levels are populated. The efficiency of the formation of highly bound molecules depends critically on the properties of the excited electronic state at intermediate distances. For homonuclear species such as Cs_2, two efficient schemes have been underlined, photoassociation toward double-well excited potentials and toward excited electronic states interacting through so-called "resonant coupling" [36]. In both cases, the density of probability in the photoassociated level presents additional maxima at intermediate or small internuclear distances, resulting in an enhancement of the stable molecule formation. The stabilized molecules are obtained in deeper vibrational levels, as observed in Rb_2 [37].

For several years, our team is analyzing theoretically, for Rb_2 and Cs_2, PA schemes using chirped laser pulses [38–40]. In the resonantly coupled 0_u^+ system of Rb_2, the coherent free evolution of the population after the end of the photoassociating pulse has been analyzed in detail in order to optimize the stimulated radiative stabilization step [41,42] in a two-color pump-dump experiment [43]. In a near future, we plan to design schemes using femtosecond chirped pulses or trains of coherent femtosecond pulses for producing translationally cold $v''=0$ ground-state RbCs molecules. Photoassociation of ultracold Rb and Cs atoms followed by spontaneous or stimulated radiative stabilization would produce stable molecules in excited levels of the X or a states. Then, a coherent population transfer converting these molecules toward the $X\ ^1\Sigma^+ v''=0$ level would be implemented. The prerequisite to this study is a detailed knowledge of the spectroscopic properties of the excited electronic states reached in the PA and RS steps or involved in the "conversion process." The motivation of the present paper is to the analyze the spin mixing in the $Rb(5s)Cs(6p_{1/2,3/2})$ 0^+ levels below the $Rb(5s)Cs(6p_{1/2})$ dissociation limit and its effects on the Franck-Condon factors (FCF). A forthcoming paper [44] will compare the properties of the $Rb(5s)Cs(6p_{1/2,3/2})$ 0^+, 0^-, and 1 levels in the same energy range and their possible contribution to efficient conversion schemes from the a state to the X state, forming RbCs molecules in the absolute ground level.

The detailed analysis of the sometimes subtle manifestations of the coupling in the 0^+ system is of a particular interest. Indeed, the $Rb(5s)Cs(6p)$ 0^+ coupled states result, in the diabatic picture, from the strong coupling of the $Rb(5s)Cs(6p)$ Hund's case a (or "diabatic") $A\ ^1\Sigma^+$ and $b\ ^3\Pi$ electronic states through electronic spin-orbit interaction. Consequently, electric dipole transitions connecting the 0^+ states to either the X or the a states contribute to the PA and RS processes and efficient spin-changing population transfer from the state a (X) to the state X (a) through the 0^+ state is expected. Furthermore, in the adiabatic description, the radial nonadiabatic coupling between Hund's case c (or "adiabatic") $0^+(P_{1/2})$ and $0^+(P_{3/2})$ electronic states is a typical example of the so-called resonant coupling [45]. Its influence is crucial to determine the efficiency of the four possible paths allowed for the PA followed by RS steps and to predict the vibrational population distribution of deeply bound stable molecules for the two isotopomers $^{85}Rb^{133}Cs$ and $^{87}Rb^{133}Cs$ [46]. A comparison with homonuclear molecules allows us to underline the specific behavior of heteronuclear species. In addition, whereas the radial coupled Schrödinger equations describing the 0^+ system are solved in the diabatic basis, the resonant coupling effects are better analyzed using a description in the adiabatic basis. To obtain quantitative information on the nonadiabatic coupling and on the adiabatic channel mixing, we introduce explicitly the "adiabatization transformation" in the two-state configuration space. It is emphasized that the analysis presented here provides the general rules for the study of resonant coupling in any homonuclear or heteronuclear species. Some results presented here have already been discussed [46]. In the latter paper, analysis of the resonant coupling in the RbCs molecule was a prerequisite to the optimization of a two-color pump-dump scheme.

The paper is organized as follows. In Sec. II, we discuss the model used to calculate the FCFs in the diabatic representation of the 0^+ states. In Sec. III A, we define the adiabatic representation. The nonadiabatic couplings are discussed in Sec. III B. We analyze the manifestations of the resonant coupling in the spectroscopic as well as in the dynamical properties of the vibrational levels of the 0^+ coupled system: distribution of vibrational levels and isotopic effect (Sec. III C), spatial localization of wave functions (Sec. III D) and FCFs for photoassociation (Sec. III E) and radiative stabilization (Sec. III F). In Sec. IV, we finally analyze the vibrational distribution of stable molecules in the $X\ ^1\Sigma^+$ and $a\ ^3\Sigma^+$ electronic states after photoassociation followed by radiative stabilization.

II. MODEL

A. Photoassociation and radiative stabilization

In photoassociation, two free colliding cold atoms resonantly absorb one photon from a cw laser red detuned by Δ_L with respect to the atomic resonance line and produce a molecule in a well-defined vibrational level $|ev'\rangle$ of an excited electronic state e. Within the Franck-Condon picture, PA is considered as a resonant vertical transition at the classical outer turning point (Condon point) of the photoassociated level, i.e., at the internuclear distance R_C^{out} where the photon energy matches the difference between the energy $\epsilon \sim 0$ of the scattering state $|g\epsilon\rangle$ describing the two colliding atoms in the ground electronic state g and the energy of the $|ev'\rangle$ level. The PA probability, proportional to $\langle g\epsilon|D(R)|ev'\rangle^2$

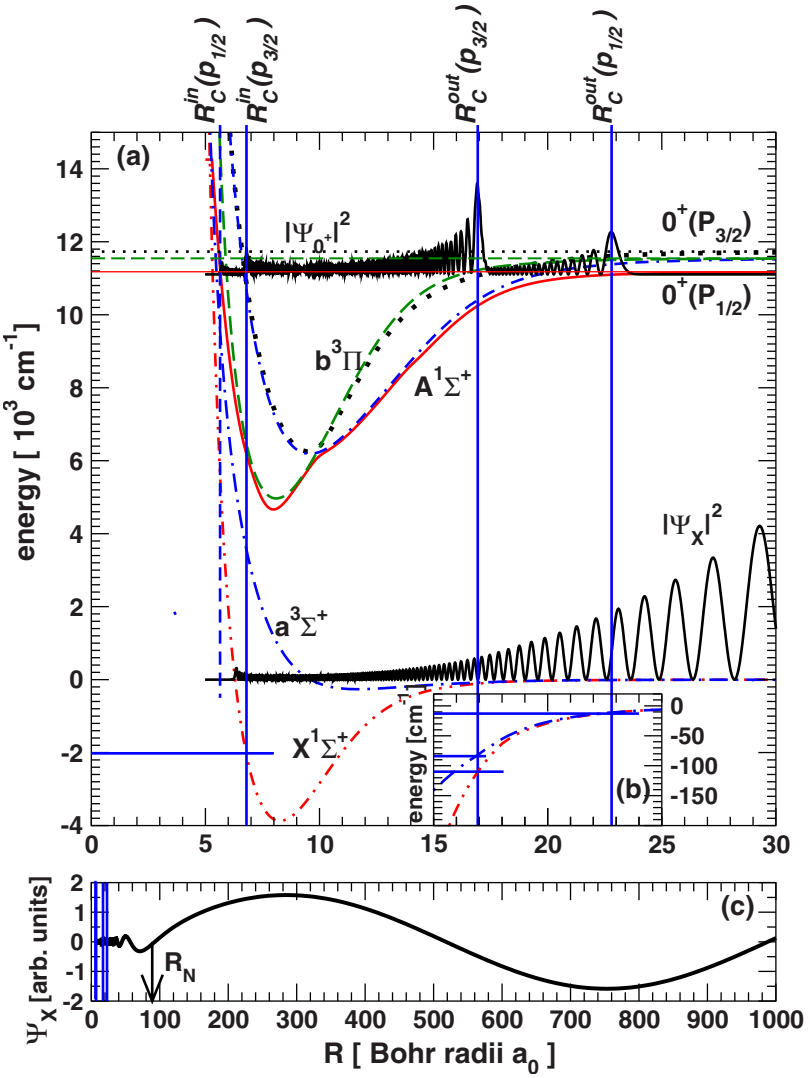

FIG. 1. (Color online) Photoassociation and radiative stabilization in RbCs: (a) Ground-state potentials $a\ ^3\Sigma^+$ (blue dot-dashed line) and $X\ ^1\Sigma^+$ (red double-dot dashed line) converging to the Rb(5*s*)Cs(6*s*) dissociation limit at 0 cm^{-1}. Diabatic excited state potentials $A\ ^1\Sigma^+$ (blue dot double-dashed line) and $b\ ^3\Pi$ (green long-dashed line) converging toward the Rb(5*s*)Cs(6*p*) threshold located at 11 547.65 cm^{-1} (horizontal green dashed line). Adiabatic potentials $0^+(P_{1/2})$ (red thin solid line) and $0^+(P_{3/2})$ (black heavy-dotted line) converging toward the two Rb(5*s*)Cs($6p_{1/2,3/2}$) limits, split by 554 cm^{-1} and indicated by the horizontal red continuous and black dotted lines. The Rb(5*s*)Cs($6p_{1/2}$) limit is located 369.406 cm^{-1} below the Rb(5*s*)Cs(6*p*) limit. Density of probability (black continuous lines) in the isotopomer ^{85}Rb^{133}Cs for a particular vibrational level, $|V'_+\rangle$ see Table I, located 72.2 cm^{-1} below the Rb(5*s*)Cs($6p_{1/2}$) limit, and for the initial scattering state $X\ ^1\Sigma^+$ with a collision energy E_i, with E_i/k_B=75 μK. The base line of each density of probability corresponds to its energy. The long-range behavior at $R>R_N$ =89a_0 (see text) of this scattering wave function is presented in (c). The three different types of stabilization at the inner $R_C^{in}(p_{3/2})$ or the outer $R_C^{out}(p_{1/2,3/2})$ [see inset (b)] turning points of the $|0^+v'\rangle$ level in the adiabatic potentials are symbolized by vertical continuous lines. Stabilization at $R_C^{in}(p_{1/2})$ is not possible, as indicated by the vertical dashed blue line.

[$D(R)$ is the electronic transition dipole moment], is approximately equal to $D(R_C^{out})^2\langle g\epsilon|ev'\rangle^2$, where $\langle g\epsilon|ev'\rangle^2$ denotes the FCF. Radiative stabilization generally occurs at the inner Condon point R_C^{in} of the $|ev'\rangle$ level. The efficiency of the formation of stable molecules can be estimated from the FCFs $\langle gv''|ev'\rangle^2$ involving the photoassociated level and bound vibrational levels $|gv''\rangle$ of the ground electronic state.

Efficient PA and RS processes require a large density of probability at R_C^{out} and at R_C^{in}, both in the ground state ($|g\epsilon\rangle$ and $|gv''\rangle$) and in the excited state $|ev'\rangle$ wave functions. In homonuclear and heteronuclear alkali-metal dimers, ground-state potentials are dominated at large distance by the van der Waals interaction, proportional to $1/R^6$. Two different behaviors, roughly limited by a characteristic position R_N (depending on the C_6 van der Walls coefficient and on the scattering length a_{SL} [40]), are observed in the $|g\epsilon\rangle$ wave function. For $R<R_N$ it oscillates rapidly with a small amplitude, the ϵ-independent nodal structure being determined by the potential energy $-C_6/R^6$, and for $R>R_N$ it presents slow oscillations with a large amplitude governed by the kinetic energy. For the ^{85}Rb^{133}Cs molecule, using C_6=5284 au [47] and a_{SL}=−1.87a_0 for the X state, one obtains R_N=89.2a_0. A smaller value R_N=69.5a_0 is obtained for the ^{85}Rb$_2$ molecule using the C_6 and a_{SL} values of Ref. [48]. In heteronuclear (homonuclear) molecules, because of the short-range character $\propto 1/R^6$ (much larger range $\propto 1/R^3$) of the excited potential, low (much larger) PA rates are observed, PA occurring at $R<R_N$ ($R\gtrsim R_N$). In contrast, the similar $1/R^6$ asymptotic behavior of the ground and excited potentials in heteronuclear systems favors the RS process [49] toward deeply bound vibrational levels.

The main characteristics of the potential curves and wave functions involved in PA and RS through the coupled 0^+ electronic states in the ^{85}Rb^{133}Cs molecule are presented in Fig. 1. The vibrational level $|V'_+\rangle$ is the level with the largest $0^+(P_{3/2})$ adiabatic component in the energy-domain experimentally investigated in Refs. [50,51]. Photoassociation occurs at the outer turning point of the $V_{1/2}$ adiabatic potential [$R_C^{out}(p_{1/2})\sim 23a_0<R_N$]. The presence in the wave function of four maxima, located at the inner and outer turning points of the two adiabatic potentials, is a signature of the resonant coupling. Three main types of stabilization populating bound levels of the X or a electronic states are expected. At large distance, around $R_C^{out}(p_{1/2})$, RS populates levels very close to the dissociation limit. Lower (a or X) levels can be populated through RS at intermediate distance $\sim R_C^{out}(p_{3/2})$ [36]. In ad-

dition, tightly bound levels of the X state are populated at short distance $\sim R_C^{in}(p_{3/2})$, i.e., at the inner turning point of the $V_{3/2}$ potential, which has at this internuclear distance a nearly pure $A\ ^1\Sigma^+$ singlet character [52]. Note that no vertical transition is possible at $R_C^{in}(p_{1/2})$, which is smaller than the R domain corresponding to the binding parts of the X and a potentials.

B. Diabatic description of the coupled system

The hyperfine interaction is neglected. Indeed, the 0^+ levels have no observable hyperfine structure [50] and we are interested in the formation of stable X and a molecules with binding energies $|E_{v''}|$ much larger than the ground-state hyperfine splitting and in photoassociated levels with binding energy of several wavenumbers. We also suppose that only s waves contribute to the PA reaction and we neglect the rotational structure.

The X and a electronic states are described in a single channel picture, with Hamiltonian $\hat{H}_i=\hat{T}_N+V_i(R)$. $V_i(R)$ ($i=X$ or a) is the Born-Oppenheimer diabatic potential involving electrostatic interactions, μ is the reduced mass, and $\hat{T}_N$ is the nuclear kinetic-energy operator, $\hat{T}_N=-(\hbar^2/2\mu)[(\partial^2/\partial R^2)+(2/R)(\partial/\partial R)]$.

In the two-channel diabatic representation of the 0^+ states, the resonant coupling [36,45,53,54] results from the spin-orbit electronic interaction $W_{\mathrm{SO}}^j(R)$, with diagonal (j=dia) and off-diagonal (j=off) terms, coupling Hund's case a electronic states $A\ ^1\Sigma^+$ and $b\ ^3\Pi$,

$$\hat{H}_e=\begin{pmatrix}\hat{T}_N+V_b(R)-W_{\mathrm{SO}}^{dia}(R) & W_{\mathrm{SO}}^{off}(R)\\ W_{\mathrm{SO}}^{off}(R) & \hat{T}_N+V_A(R)\end{pmatrix}. \quad (1)$$

The decomposition of the $|0^+v'\rangle$ levels, labeled according to increasing energy $E_{v'}$ [with $E_{v'}=0$ at the Rb($5s$)Cs($6p_{1/2}$) limit], on the two diabatic electronic channels with electronic wave functions $|b\rangle$ and $|A\rangle$ (depending on the electronic variables and on the internuclear distance R) writes

$$|0^+v'\rangle=\frac{1}{R}\Psi_b^{v'}(R)|b\rangle+\frac{1}{R}\Psi_A^{v'}(R)|A\rangle, \quad (2)$$

The diabatic vibrational wave functions $\Psi_b^{v'}(R)$ and $\Psi_A^{v'}(R)$ solutions of the coupled radial equations resulting from Eq. (1) satisfy $\int_0^\infty[(\Psi_b^{v'})^2+(\Psi_A^{v'})^2]dR=1$. Information on the radial localization of the density of probability can be obtained from the rotational constant,

$$B_{v'}=\langle 0^+v'|\hbar^2/(2\mu R^2)|0^+v'\rangle = \int_0^\infty \frac{\hbar^2}{2\mu R^2}[(\Psi_b^{v'})^2+(\Psi_A^{v'})^2]dR. \quad (3)$$

Levels associated with large $B_{v'}$ values correspond to a small elongation of the atom pair.

The Hamiltonians are represented using the mapped Fourier grid Hamiltonian method [55]. The extension of the box, $L=17\,000a_0$, is sufficiently large to allow a reliable description of scattering states with collision energy, $E=k_BT$, in the μK range (k_B is the Boltzmann constant). The step of the grid is adjusted to the local de Broglie wavelength allowing the reduction in the number of points down to $N\approx 1000$ [55,56]. Rather than the usual plane-wave expansion (Fourier expansion), we use basis sine functions with zero boundary condition [56], which is one of the various methods developed to eliminate ghost states [57].

Electric dipole transitions toward $|0^+v'\rangle$ levels are allowed from both the $|X\ ^1\Sigma^+v''\rangle$ and the $|a\ ^3\Sigma^+v''\rangle$ levels. Due to the spin selection rule, the radial matrix element for the electronic transition dipole moment $\langle 0^+v'|D(R)|iv''\rangle$, with $i=X$ ($i=a$) involves only the component $\Psi_j^{v'}$ $j=A$ ($j=b$) of the $|0^+v'\rangle$ wave function. Neglecting here the R variation in $D(R)$, the above matrix element is proportional to overlap integrals.

C. Potentials

For the X and a potentials, we use at short and intermediate distances the *ab initio* potentials constructed by Allouche *et al.* [58]. These potentials are connected to the multipolar expansion describing the long-range interaction $C_6/R^6+C_8/R^8+C_{10}/R^{10}$ with the C_n coefficients found in [47]. A smooth matching was achieved at $R=15.3a_0$ including the exchange potentials given as form I in Table 2 of Ref. [59]. In order to better describe the collisional properties, we have slightly modified the repulsive wall of the potentials to match the observed scattering length a_{SL} in the potential $a\ ^3\Sigma^+$ for the ^{87}RbCs molecule [60]. The a_{SL} values used here are $14.28a_0$ ($-1.87a_0$) for the $X\ ^1\Sigma^+$ potential of ^{87}RbCs (^{85}RbCs) and $710a_0$ ($18.72a_0$) for the $a\ ^3\Sigma^+$ potential of ^{87}RbCs (^{85}RbCs).

The potentials $V_i(R)$ ($i=A,b$) and the spin-orbit coupling functions $W_{\mathrm{SO}}^j(R)$ have been obtained by Bergeman *et al.* [61–63] making use of the spectral transitions observed by DeMille and combining them with *ab initio* calculations [58,64]. These potentials have been connected to the asymptotic expansions including the C_6 and C_8 terms [47] at $R=24.17a_0$ and $23.07a_0$ for the V_A and V_b potentials, respectively.

III. RESONANT COUPLING

In our calculations, the coupled levels $|0^+v'\rangle$ are obtained in Hund's case a representation using the basis of the diabatic electronic wave functions $|A\rangle$ and $|b\rangle$. In heavy species such as Rb_2 or RbCs, because of the large value of the fine structure splitting, the vibrational levels of the 0^+ coupled system are more suitably analyzed in Hund's case c representation by decomposing the coupled wave functions $|0^+v'\rangle$ on the basis of adiabatic electronic wave functions $|P_{1/2,3/2}\rangle$ [65]. The two-channel transformation from diabatic to adiabatic representation is summarized in Appendix A 1. The radial nonadiabatic coupling operators are determined in Appendix A 2.

A. Adiabatic electronic potentials

The properties of the adiabatic electronic states $0^+(P_{1/2,3/2})$ and of their vibrational levels, the "pure adiabatic levels" $|P_{1/2,3/2}v_{\mp}\rangle$ [see Eq. (A2)] are analyzed in this

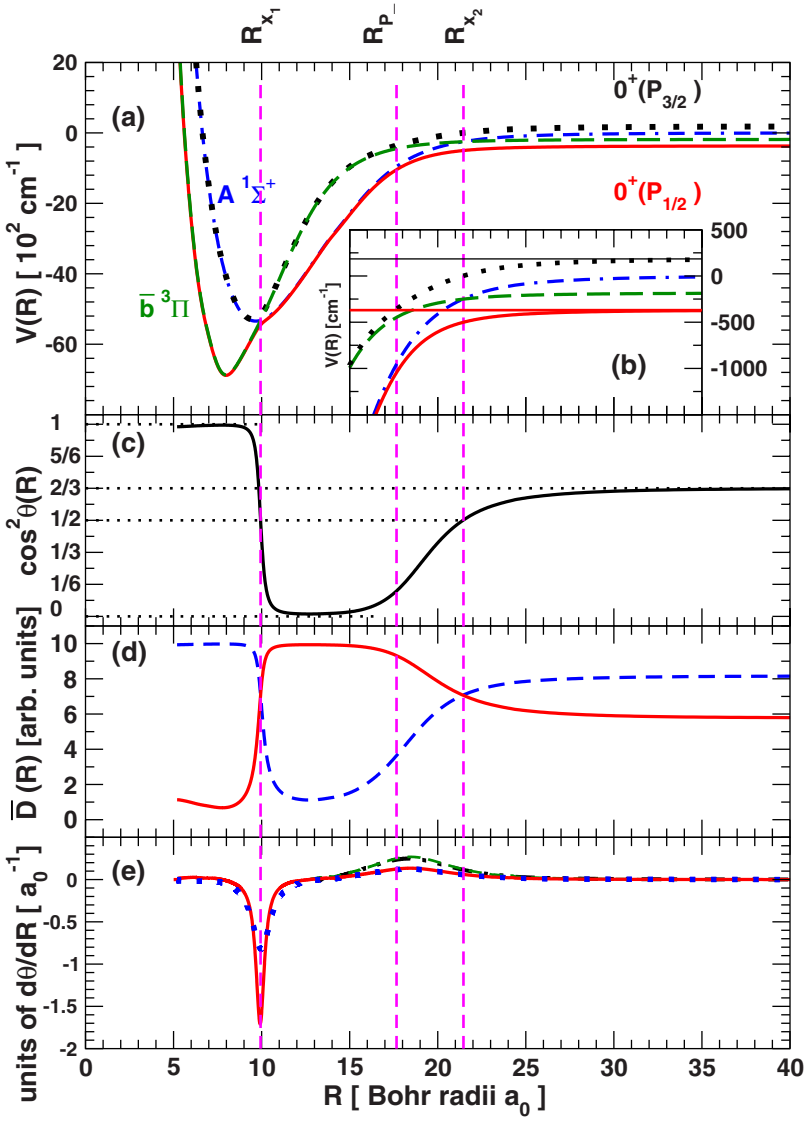

FIG. 2. (Color online) Resonant coupling in 0^+ electronic states: potentials and couplings. (a) diabatic potentials $V_A(R)$ and $V_{\bar{b}}(R)$ of the states $A\,^1\Sigma^+$ (blue dot double-dashed line) and $\bar{b}\,^3\Pi$ (green long-dashed line), including the diagonal part of the spin-orbit coupling [notice the two crossings at R_{x_1} and R_{x_2} detailed in inset (b)], and adiabatic potentials $V_{1/2}$ and $V_{3/2}$ of the states $0^+(P_{1/2})$ (red continuous line) and $0^+(P_{3/2})$ (black dotted line). (b) The $V_{3/2}$ potential connected to the $\mathrm{Rb}(5s)\mathrm{Cs}(6p_{3/2})$ dissociation limit at 185 cm^{-1} (horizontal black thin line) crosses the $\mathrm{Rb}(5s)\mathrm{Cs}(6p_{1/2})$ dissociation limit located at -369.4 cm^{-1} (horizontal red heavy line) at R_{P_-}. (c) R-dependent spin character of the adiabatic electronic states [Eqs. (A1)]; variation with R of $\cos^2\theta$, θ being the rotation angle between diabatic and adiabatic channels. (d) Electronic transition dipole moment $\bar{D}(R)$ for excitation from $X\,^1\Sigma^+$ state toward adiabatic states $0^+(P_{1/2})$ (full red line) and $0^+(P_{3/2})$ (blue dashed line) or from $a\,^3\Sigma^+$ toward $0^+(P_{1/2})$ (blue dashed line) and $0^+(P_{3/2})$ (full red line) in arbitrary units and assuming no R dependence for the electronic transition dipole moment $D(R)$ between diabatic states. (e) Nonadiabatic coupling [Eq. (A4)]; variation with R of $\partial\theta/\partial R$ either for a R-dependent spin-orbit coupling [61] (red continuous line) or for a constant spin-orbit coupling fixed to its asymptotic value (blue dotted line). Around R_{x_2} the couplings, multiplied by a factor of 5, are represented by the green long-dashed and black double-dot dashed lines.

section. The upper panel of Fig. 2 presents the two diabatic potentials $V_A(R)$ and $V_{\bar{b}}(R)=V_b(R)-W_{\mathrm{SO}}^{dia}(R)$, the latter potential including the diagonal part of the spin-orbit interaction. These diabatic potentials present two crossings, the first at short distance $R_{x_1}=9.94a_0$ and the second at larger distance $R_{x_2}=21.46a_0$ [see Fig. 2(b)]. The two adiabatic potentials $V_{1/2}$ and $V_{3/2}$, deduced from V_A and $V_{\bar{b}}$ by the rotation $\theta(R)$, converge toward the two dissociation limits $\mathrm{Rb}(5s)\mathrm{Cs}(6p_{1/2,3/2})$ and present two anticrossings [see Fig. 2(a)]. The R variation in $\cos^2\theta$, i.e., of the weight of the triplet (singlet) component in the $0^+(P_{1/2})$ $[0^+(P_{3/2})]$ electronic channel, is presented in Fig. 2(c). It is equal to $1/2$ at the two crossings R_{x_i}. The lowest adiabatic channel $0^+(P_{1/2})$ presents a predominant triplet character both at short ($R<R_{x_1}$) and at large ($R>R_{x_2}$) internuclear distances. There is a steplike variation in the spin character of the adiabatic electronic channels for $R\sim R_{x_1}$, where the diabatic curves cross each other abruptly. For $R\gtrsim 17a_0$, $\cos^2\theta$ increases slowly toward $2/3$, the anticrossing at R_{x_2} being not precisely localized. This anticrossing controls the properties of the coupled 0^+ levels and FCFs close to the $\mathrm{Rb}(5s)\mathrm{Cs}(6p_{1/2})$ threshold (see Sec. III E).

In the adiabatic single-channel representation of the excited electronic states, there is a strong R dependence of the electronic dipole transition moment $\bar{D}(R)$ for excitation of the $0^+(P_{1/2})$ state either from the X state $[\bar{D}(R)=D\sin\theta(R)]$ or from the a state $[\bar{D}(R)=D\cos\theta(R)]$ [see Fig. 2(d)]. Similar dipole moments are obtained for the excitation of the $0^+(P_{3/2})$ state from the a state or from the X state. For each adiabatic level $|P_{1/2}v_-\rangle$ ($|P_{3/2}v_+\rangle$), it is possible to determine, at the Condon point $R_C^{in,out}(p_{1/2})$ $[R_C^{in,out}(p_{3/2})]$, the triplet (singlet) character of the $0^+(P_{1/2})$ $[0^+(P_{3/2})]$ electronic channel, and to infer the stable state (a or X) preferentially populated by RS from this level. In particular, the potential $V_{3/2}$ crosses the dissociation limit $\mathrm{Rb}(5s)\mathrm{Cs}(6p_{1/2})$ at $R_{P_-}=15.57a_0<R_{x_2}$, where $\cos^2\theta(R_{P_-})=0.125$ is much smaller than $1/2$. Therefore, in this energy range, the wave functions of pure adiabatic levels possess, at their outer Condon point, a predominant $b\,^3\Pi$ character, with a weight equal to $2/3$ (0.875) for the levels $|P_{1/2}v_-\rangle$ ($|P_{3/2}v_+\rangle$), which favors PA and RS processes from and toward the a triplet state (see Sec. IV). We emphasize that the previous weights being evaluated at different positions, re-

spectively $R \sim \infty$ and $(R=R_{P\_})$, there is no relation between them.

The wave functions for the pure adiabatic vibrational levels have very different spatial extensions: the $|P_{1/2}v_-\rangle$ levels have a broad extension, from $R_C^{in}(p_{1/2})$ to $R_C^{out}(p_{1/2})$, meanwhile the $|P_{3/2}v_+\rangle$ wave functions are located in a reduced spatial range, $R_C^{in}(p_{3/2})$ to $R_C^{out}(p_{3/2})$. Decomposing these wave functions in the diabatic basis using Eqs. (A1), the steplike variation in $\cos\theta(R)$ at R_{x_1} curves out a "hole" in the $b\,^3\Pi$ $(A\,^1\Sigma^+)$ diabatic radial component $\varphi_{1/2}^{v_-}(R)\cos\theta(R)$ $[\varphi_{3/2}^{v_+}(R)\cos\theta(R)]$ of the $|P_{1/2}v_-\rangle$ $(|P_{3/2}v_+\rangle)$ level which extends in two distinct spatial domains $R<R_{x_1}$ and from $R \sim R_{x_2}$ to $R_C^{out}(p_{1/2})$ $[R_C^{out}(p_{3/2})]$. In the diabatic representation of the 0^+ coupled states, the observation in the wave functions of a similar switchover from singlet to triplet character around R_{x_1} allows one to conclude that nonadiabatic couplings are negligible. Such an argument has been used in Ref. [46] to demonstrate qualitatively in RbCs that introducing spin-orbit functions W_{SO}^j fixed to their asymptotic values leads to a near-adiabatic 0^+ system (see Fig. 9 of that paper). A quantitative evaluation of the adiabatic $0^+(P_{1/2,3/2})$ channel mixing in the $|0^+v'\rangle$ coupled levels is obtained quantitatively in the present paper from the norm of the adiabatic vibrational wave functions $\Psi_{1/2,3/2}^{v'}(R)$ [see Eq. (A3)].

B. Adiabatic analysis of the coupled system

Analytical formulas for the radial coupling between adiabatic electronic states in Hund's case *c* description of the 0^+ system are derived in Appendix A 2 without neither introducing the electronic wave functions $\{|A\rangle,|b\rangle\}$ or $\{|P_{1/2}\rangle,|P_{3/2}\rangle\}$ nor their derivatives.

The nonadiabatic coupling is larger near the crossing points R_{x_i} of the diabatic potentials, where it is equal to $a_i/4W_{\mathrm{SO}}^{off}(R_{x_i})$ [a_i is the slope of the vertical separation between the two potentials see Eqs. (A4) and (A5)]. As shown in Fig. 2(e), the first contribution $\partial\theta/\partial R$ to the radial coupling is very weak around R_{x_2} and much larger around R_{x_1}, especially when a *R*-dependent spin-orbit coupling [63] is considered (see Fig. 2 in Ref. [46]). In the contribution $\partial^2\theta/\partial R^2$ [see Eq. (A4)] the *R* dependence, shaped like a dispersion curve, introduces cancellation effects. In all the cases encountered in our study, this second contribution is smaller than the first one by one order of magnitude.

Whereas the spin-orbit interaction between Hund's case *a* electronic states is completely delocalized in the *R* domain, the nonadiabatic coupling between Hund's case *c* states is strongly localized at short range, around R_{x_1}, where the energy dependence of the adiabatic radial wave functions is given by the normalization factor, i.e., by the density of states in the $0^+(P_{1/2,3/2})$ channels. Therefore, the matrix element $\langle P_{1/2}v_-|\hat{T}_N|P_{3/2}v_+\rangle$ varies slowly with v_- and v_+. The multichannel quantum defect theory (MQDT) [54,66,67], which introduces the adiabatic channels $0^+(P_{1/2,3/2})$ and the short range interaction localized around R_{x_1}, would be suitable for describing the coupled 0^+ levels. However, the interest of this method is in practice limited by the strong energy dependence of the MQDT parameters [68]. It is recalled that such a global description of channel coupling, more appropriate than a detailed local description in terms of mixing between individual levels, is at the origin of the name "resonant coupling" [45,54].

The matrix element [see Eq. (A4)] of the nonadiabatic coupling depends on the overlap of the vibrational wave functions $\varphi_{1/2,3/2}^{v_\mp}$, more specifically on their relative phase in the range $R \sim R_{x_1}$. Considering the first term in Eq. (A4), maximum level mixing is obtained when the two wave functions oscillate with phases differing by $\pi/2$ at this distance. In the WKB description of the wave functions, the local difference of the phases of the wave functions at R_{x_1} is equal to the difference of the classical actions, calculated in the two adiabatic potentials between the inner turning point and R_{x_1}. These quantities depend on the local de Broglie wavelength and therefore on the reduced mass [69], which explains the spectacular isotopic effect discussed in the next paragraph.

C. Irregularities in the 0^+ states: Isotopic effect

In this section, we discuss the irregularities observed in the rotational constants $B_{v'}$ [see Eq. (3)] [53] of the 0^+ levels due to the channel mixing (either in Hund's case *a* or in Hund's case *c* descriptions).

Figure 3 presents the variation in $B_{v'}$ as a function of the energy of the coupled levels of the two molecules ^{85}RbCs and ^{87}RbCs. The "resonant" behavior of this quantity, with abrupt oscillations, is due to the presence of two series with different properties. Levels with the largest $B_{v'}$ values have wave functions strongly localized at short internuclear distance, i.e., possess the largest $0^+(P_{3/2})$ weight [see Eq. (A3)].

For the studied levels, $R_C^{out}(p_{3/2})$ varies from $16.27a_0$ to $17.57a_0$ and, at this distance, the $b\,^3\Pi$ character of the $0^+(P_{3/2})$ state is very large, decreasing from 95% to 87.5% [see Fig. 2(c)]. Consequently, levels with a high $0^+(P_{3/2})$ character, and therefore an important density of probability around $R_C^{out}(p_{3/2})$, possess a strong $b\,^3\Pi$ character (see in Fig. 3). On the other hand, for levels with $E_{v'}>-130$ cm^{-1}, the $b\,^3\Pi$ character of the $0^+(P_{1/2})$ state at $R_C^{out}(p_{1/2})$ increases from 50% to 66%. The predominant $b\,^3\Pi$ character of these 0^+ levels explains the large distribution of population in the $a\,^3\Sigma^+$ state after PA and RS (see Sec. IV A).

Very different behaviors are observed in the two isotopomers. For ^{85}RbCs, well pronounced oscillations occur, the coupled $|0^+v'\rangle$ levels with a large $(>80\%)$ $0^+(P_{1/2})$ character being easily identified. For the ^{87}RbCs, the effects due to the nonadiabatic couplings are stronger: the oscillations are very smooth and the $0^+(P_{3/2})$ character is spread across a large number of $|0^+v'\rangle$ levels. For the two isotopomers, the coupling between the two adiabatic channels is described by the same *R* variation in the θ angle. However, the importance of the cancellation effects occurring in the integrals involving the $\varphi_{1/2}^{v_-}$ and $\varphi_{3/2}^{v_+}$ adiabatic vibrational functions [see Eq. (A4)] is very different for the two isotopomers.

Comparative experimental study of ultracold ground-state molecule formation in the $^{85}Rb_2$ and $^{87}Rb_2$ isotopomers has been recently presented [71]; most differences were ascribed

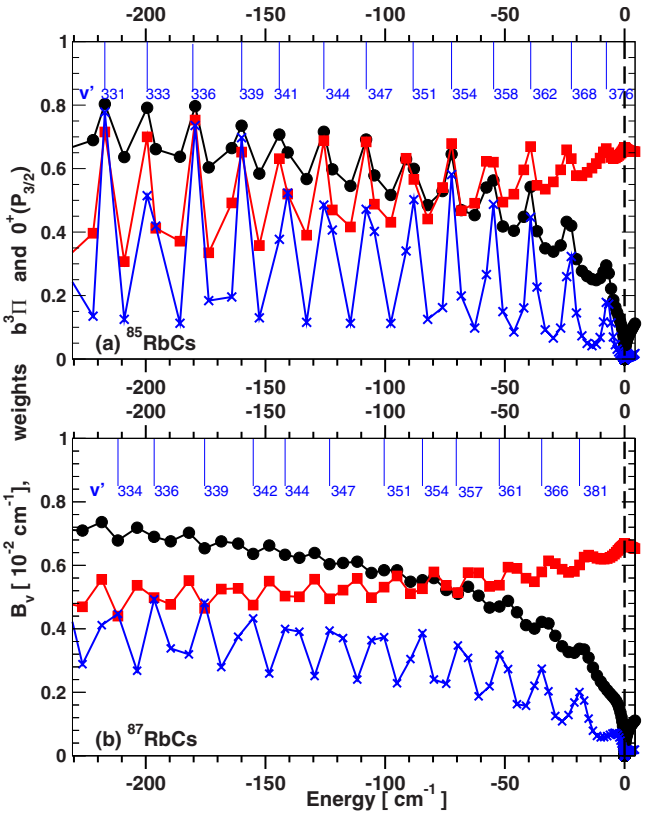

FIG. 3. (Color online) Irregularities in the 0^+ spectra and isotopic effect. For the two isotopes, (a) ^{85}RbCs and (b) ^{87}RbCs, variations as a function of the energy $E_{v'}$ (in cm^{-1}) of the $|0^+v'\rangle$ level of the rotational constant $B_{v'}$ (in units of 10^{-2} cm^{-1}, black circle), of the weight of the $b\,^3\Pi$ diabatic state (red square), and of the weight of the $0^+(P_{3/2})$ adiabatic state (blue cross). The Rb(5s)Cs(6$p_{1/2}$) dissociation limit is indicated by the vertical black dashed line. The vertical blue segments indicate the quantum numbers v' of the $|0^+v'\rangle$ levels with the largest $0^+(P_{3/2})$ weight.

to isotopic effect in the resonant coupling in the photoassociated 0_u^+ coupled states.

D. Wave functions

The wave functions of the 0^+ coupled levels are analyzed both in Hund's case a and in Hund's case c descriptions to obtain information on the most efficient stabilization processes and on the R localization of nonadiabatic couplings, respectively.

Two typical examples are presented in Fig. 4 for the ^{85}RbCs molecule: the $|0^+v'=354\rangle$ level with a dominant $0^+(P_{3/2})$ character, noted by $|V'_+\rangle$, and the nearly pure $0^+(P_{1/2})$ level with $v'=360$, noted $|V'_-\rangle$. Both levels have a predominant $b\,^3\Pi$ character, especially the $|V'_+\rangle$ level. The characteristics of these levels are reported in Table I.

For both levels, the total density of probability [panels (a)] extends from $R_C^{in}(p_{1/2})$ to $R_C^{out}(p_{1/2})$ and presents four maxima at the inner and outer turning points of the adiabatic potentials $V_{1/2}$ and $V_{3/2}$, which is a manifestation of the nonadiabatic effects. The maximum of the density probability at $R_C^{out}(p_{3/2})$ is well pronounced for $|V'_+\rangle$ and almost unnoticeable for $|V'_-\rangle$.

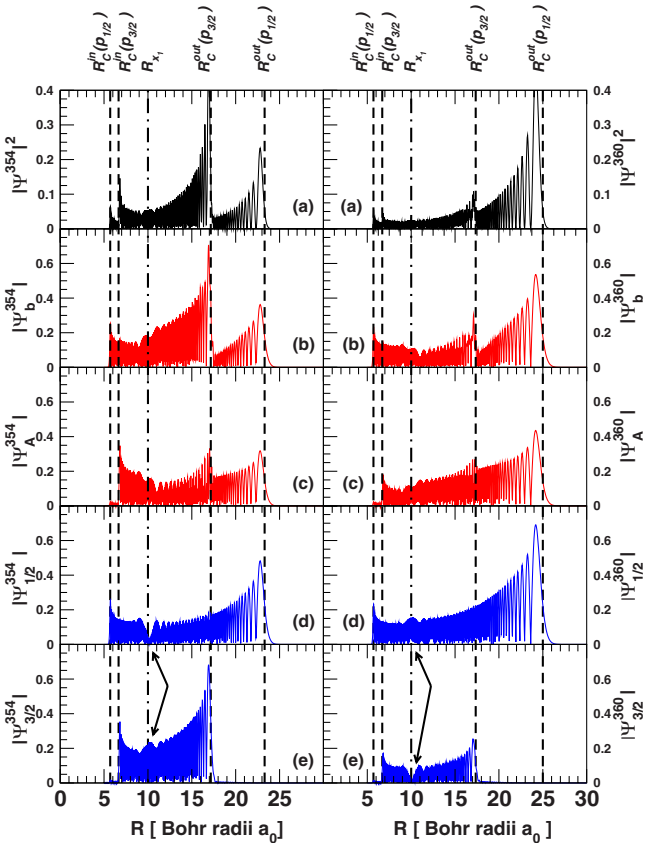

FIG. 4. (Color online) Wave functions for the $|V'_+\rangle$ (left column) and $|V'_-\rangle$ (right column) $|0^+v'\rangle$ levels in ^{85}RbCs (see Table I). Panel (a): total density of probability. Panels (b) and (c): diabatic vibrational radial wave functions $|\Psi_b^{v'}|$ and $|\Psi_A^{v'}|$. Panels (d) and (e): adiabatic vibrational radial wave functions $|\Psi_{1/2}^{v'}|$ and $|\Psi_{3/2}^{v'}|$. Maxima of the total density of probability occur at the inner and outer Condon points $R_C^{in,out}(p_{1/2,3/2})$ of the adiabatic potentials $V_{1/2,3/2}$. Nonadiabatic radial couplings between the adiabatic components induce destructive or constructive interference effects (black arrows) at the crossing point R_{x_1} of the diabatic potentials $V_A(R)$ and $V_{\bar{b}}(R)$.

In the Hund's case a basis representation, the diabatic radial wave functions $\Psi_{A,b}^{v'}$ [panels (b) and (c) of Fig. 4] present a very irregular behavior with a noticeable amplitude increase at $R_C^{out}(p_{3/2})$. They cover the complete R domain up to $R_C^{out}(p_{1/2})$, where the adiabatic electronic wave function $|P_{1/2}\rangle$ corresponds to a strong mixing of $|A\rangle$ and $|b\rangle$ diabatic electronic wave functions. For both 0^+ levels, the wave function $\Psi_A^{v'}$ with a low amplitude for $R_C^{in}(p_{1/2}) \leqslant R < R_C^{in}(p_{3/2})$ presents a sharp increase at $R_C^{in}(p_{3/2})$, where the $0^+(P_{3/2})$ adiabatic state changes into an almost pure $A\,^1\Sigma^+$ diabatic state. As shown in Sec. IV A, this explains, especially for the $|V'_+\rangle$ level, the large value of the RS probability toward low lying levels of the ground X state through vertical transitions around $R_C^{in}(p_{3/2})$. The absence of drastic change in the amplitudes of $\Psi_{A,b}^{v'}(R)$ at R_{x_1} is a signature of the large nonadiabatic coupling effects (see Sec. III A).

The relative weight of the two $0^+(P_{1/2,3/2})$ channels can be deduced from Hund's case c representation of the wave func-

TABLE I. Spectroscopic and dynamical properties of two typical $|0^+v'\rangle$ levels with $v'=354$ ($|V'_+\rangle$) and $v'=360$ ($|V'_-\rangle$) in ^{85}RbCs. The weights of diabatic $\{|A\rangle,|b\rangle\}$ and adiabatic $\{|P_{1/2}\rangle,|P_{3/2}\rangle\}$ electronic states are indicated (in percent) in lines 1 and 2. The detuning $\Delta_{v'}$ and the rotational constant $B_{v'}$ are reported in lines 3 and 4. The branching ratios $\bar{R}^i_j(v')$ [Eq. (4)] for radiative stabilization toward stable $i=X$ and $i=a$ electronic states are respectively reported in lines 5–9 and 10–13. The characteristics of the different types j of stabilization (specified in column 1) are presented: position R_C (in unit of Bohr radii a_0) of the Condon points in the $V_{1/2,3/2}$ potentials (columns 2 and 5), branching ratio toward bound levels in percent (columns 3 and 6), approximate energy, $E^M_{v''}\sim V_i(R_C)$ (in cm^{-1}), of the stable v'' level populated by a vertical transition at R_C (columns 4 and 7). The branching ratios for formation of molecules in bound vibrational levels (of atom pairs) in the X or a states are indicated in lines 8 and 12 (9 and 13). The branching ratio (stable molecules plus atom pairs) for molecule formation in singlet or triplet levels is equal to the weight of the $|A\rangle$ or $|b\rangle$ state in the wave function of the $|0^+v'\rangle$ level.

		$\|V'_+\rangle$			$\|V'_-\rangle$	
Channel mixing						
$\{\|A\rangle,\|b\rangle\}$	32.1	67.9		48.1	51.9	
$\{\|P_{1/2}\rangle,\|P_{3/2}\rangle\}$	41.9	58.1		91.5	8.5	
$\Delta_{v'}=\|E_{v'}\|$ (cm^{-1})		72.2			46.2	
$B_{v'}$ (10^{-2} cm^{-1})		0.646			0.404	
$X\,^1\Sigma^+$	R_C	$\bar{R}^X_j$	$E^M_{v''}$	R_C	$\bar{R}^X_j$	$E^M_{v''}$
$R^{out}_C(p_{1/2})$	23.12	4.71	−10.2	24.63	10.98	−6.8
$R^{out}_C(p_{3/2})$	17.09	4.30	−100.0	17.26	0.97	−94.0
$R^{in}_C(p_{3/2})$	6.74	1.55	−1850.0	6.73	0.22	−1800.0
Stable molecules		10.56			12.17	
Atom pairs		21.54			35.89	
$a\,^3\Sigma^+$	R_C	$\bar{R}^a_j$	$E^M_{v''}$	R_C	$\bar{R}^a_j$	$E^M_{v''}$
$R^{out}_C(p_{1/2})$	23.12	7.81	−9.9	24.63	16.78	−6.7
$R^{out}_C(p_{3/2})$	17.09	13.40	−77.4	17.26	1.91	−73.1
Stable molecules		21.21			18.69	
Atom pairs		46.69			33.25	

tions [panels (d) and (e) of Fig. 4]; $\Psi^{v'}_{1/2,3/2}(R)$ present a more regular shape and extend in different R domains, due to very different locations of the Condon points in the $V_{1/2,3/2}$ potentials. Significant constructive or destructive interference effects, observable around the inner crossing point R_{x_1} [see the arrows in Figs. 4(d) and 4(e)], are a consequence of the nonadiabatic coupling effects mainly localized at this distance.

E. Effects on photoassociation

The variation in FCF's for PA as a function of the energy $E_{v'}$ of the photoassociated levels is analyzed. The strong changes resulting from the spin-orbit coupling of the A and b states are underlined.

In ^{85}RbCs, the FCFs relevant to PA from the X state toward pure $|A\,^1\Sigma^+v'\rangle$ vibrational levels have been previously analyzed and compared with the corresponding ones in $^{85}Rb_2$ [46]. These FCFs show a typical oscillating pattern [see Figs. 5(b) and 8] reproducing the nodal structure (depending on the scattering length a_{SL}) of the scattering wave function. The very rapid oscillations close to the dissociation limit are due to the slow variation in the $V_{1/2}$ potential for $R>40a_0$. The envelope of the oscillations decreases very rapidly when $|E_{v'}|$ increases, the values of the FCF at $|E_{v'=385}|\sim 1$ cm^{-1} ($|E_{v'=391}|\sim 0.05$ cm^{-1}) being by more than one (three) order(s) of magnitude smaller than the FCFs close to threshold, at $|E_{v'=393}|\sim 0.002$ cm^{-1}. Simultaneously $R^{out}_C(p_{1/2})$ increases very rapidly, being respectively equal to $45a_0$, $80a_0$, and $130a_0$. For all $|0^+v'\rangle$ levels, except for the three upper ones below the dissociation limit, the rightmost turning point lies in the inner domain $R\leqslant R_N$, where the amplitude of the scattering wave function is small, explaining the low efficiency of the PA process. The major differences between photoassociation in heteronuclear and in homonuclear molecules consist in a smaller amplitude of the scattering wave function at $R^{out}_C(p_{1/2})$, resulting in a lower PA probability, in a shorter spacing of the oscillations and in a smaller density of excited levels. All these properties stem from the difference in the long-range tail of the excited potential. For $|E_{v'}|$ ranging from 2 to 100 cm^{-1}, the FCFs for PA from the X state are larger by a factor of 4 in ^{85}RbCs than in ^{87}RbCs; for PA from the a state, the FCFs are twice as large in ^{87}RbCs.

The originality of the present section is to show explicitly the modifications induced by the resonant coupling in the 0^+

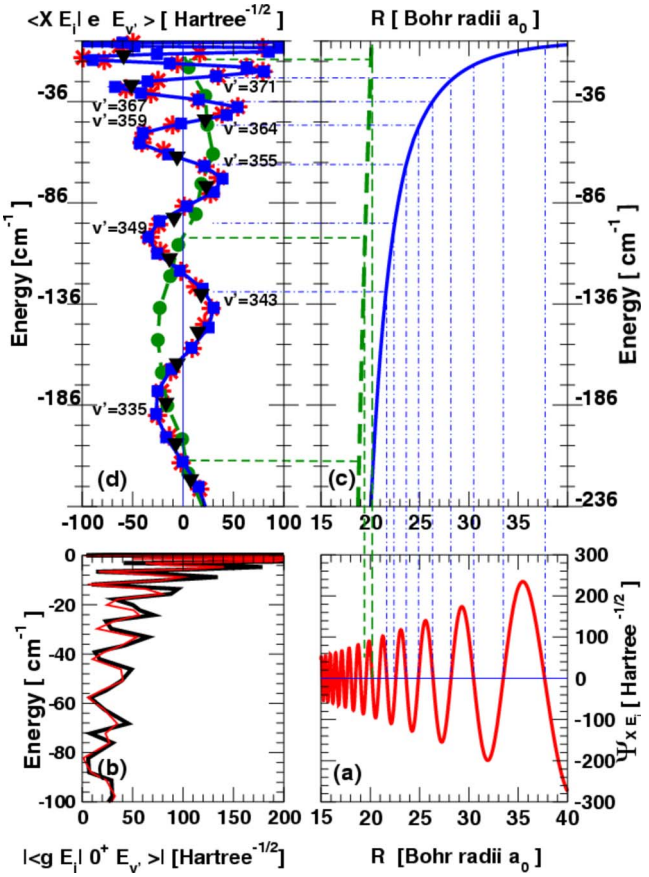

FIG. 5. (Color online) Resonant coupling in the 0^+ electronic states: effects on photoassociation. (a) Scattering wave function $|XE_i\rangle$ in the ground state of ^{85}RbCs for a scattering length $a_{SL}=14.28a_0$. The scattering wave function is energy normalized [unit (hartree)$^{-1/2}$]. (d) Overlap integral $\langle XE_i|eE_{v'}\rangle$ between $|XE_i\rangle$ and excited levels with energy $E_{v'}$; the excited levels are either pure diabatic $e=A\,^1\Sigma^+$ levels (green dot), pure adiabatic $e=0^+(P_{1/2})$ levels (blue square), or coupled $e=0^+$ levels with a predominant character either $0^+(P_{1/2})$ (red star) or $0^+(P_{3/2})$ (black triangle). The indicated v'-values correspond to extrema of the overlap integral. (c) Reflection principle either on the excited diabatic V_A (green dashed curve) or adiabatic $V_{1/2}$ potentials (blue full curve), relating the nodes in the scattering wave function to the nodes in the corresponding overlap integral. (b) Absolute value of the overlap integral between a scattering level with energy $E_i/k_B=75$ μK, either in the ground $g=X$ electronic state (full thin curve) or in the lowest triplet $g=a$ triplet state (full heavy curve), and coupled $|0^+E_{v'}\rangle$ levels.

states. In ^{85}RbCs, the variation with $E_{v'}$ of the overlap integral $\langle XE_i|eE_{v'}\rangle$ involved in PA from the X state toward excited levels with energy $E_{v'}$ is reported in Fig. 5(d) for various representations of the excited electronic states e. The oscillations do not depend on the energy E_i of the scattering state, photoassociation occurring at $R<R_N$ (see Sec. II C). The overlap integral varies slowly with $E_{v'}$ when the $|eE_{v'}\rangle$ levels are pure diabatic levels ($e=A\,^1\Sigma^+$). Much more rapid oscillations appear for pure adiabatic levels ($e=P_{1/2}$) or for coupled levels ($e=0^+$). The latter two calculations yield nearly identical results. For $|0^+v'\rangle$ levels, there is no significant difference in the PA excitation for levels with a predominant $0^+(P_{1/2})$ or $0^+(P_{3/2})$ character.

The variation with $E_{v'}$ of the FCF reflects the nodal structure of the ground-state scattering wave function [23]. From the reflection principle, the FCF vanishes when R_C^{out}, the outer Condon point of the $|eE_{v'}\rangle$ level, corresponds to a node of the scattering wave function [see Figs. 5(a) and 5(d)]. For $|E_{v'}|<200$ cm^{-1}, $R_C^{out}(p_{1/2})$ is close to R_{x_2}. Due to the crossing at large distance, the asymptotic forms of the adiabatic potentials $V_{1/2,3/2}$ differ completely from the ones of the diabatic potentials V_A and V_b. This explains the difference in the energy dependence of the various overlap integrals reported in Fig. 5(d) and the similarities in the results obtained for adiabatic $|P_{1/2}v_-\rangle$ or coupled $|0^+v'\rangle$ levels. A description of excited levels in the pure Hund case a representation which would lead to transitions $X\rightarrow A$ and $a\rightarrow b$ is not at all realistic.

Figure 5(b) summarizes the behavior of the overlap integrals relevant to PA of $|0^+v'\rangle$ levels from the stable X and a states. The nearly identical energy dependence of the two overlap integrals [Fig. 5(b)] is fortuitously due to very close values of the scattering length in the V_X and V_a potentials in ^{85}RbCs, leading to singlet and triplet scattering wave functions oscillating nearly in phase for $R\sim R_C^{out}(p_{1/2,3/2})$ ($\sim 15-40a_0$). Furthermore, photoassociation from $a\,^3\Sigma^+$ is more favorable at $|E_{v'}|<20$ cm^{-1}.

F. Effect on stabilization

We compare the stabilization processes from coupled $|0^+v'\rangle$ and diabatic $|P_{1/2,3/2}v_\mp\rangle$ levels to underline the importance of nonadiabatic couplings. In Figs. 6(a) and 6(b), the top panels display the overlap integrals $I(0,v')$ for RS from the $|V'_+\rangle$ and $|V'_-\rangle$ levels, the 0^+ coupled levels described in Table I. Overlap integrals $I(3/2,v_+)$ and $I(1/2,v_-)$ for transitions from pure $|P_{3/2}v_+\rangle$ and $|P_{1/2}v_-\rangle$ adiabatic levels with approximately the same energies as the corresponding $|0^+v'\rangle$ levels are presented in the middle and bottom panels.

Stabilization from $|P_{1/2}v_-\rangle$ adiabatic levels populates only vibrational levels bound by less than 15 cm^{-1} in both the $X(v''\geqslant 122)$ and the a state ($v''\geqslant 33$). Stabilization from $|P_{3/2}v_+\rangle$ adiabatic levels populates X levels bound by up to 2000 cm^{-1} and an enhancement of the RS probability is observed for X levels bound by $\sim 90-100$ cm^{-1}. Concerning the stabilization from $|P_{3/2}v_+\rangle$ adiabatic levels toward a levels, levels bound by $\sim 70-80$ cm^{-1} are the most efficiently populated.

Maximum values of the overlap integrals $I(0,v')$ correspond approximately to "vertical" transitions, when they exist, at the inner and outer turning points $R_C^{in,out}(p_{1/2,3/2})$ of the adiabatic $V_{1/2,3/2}$ potentials, where the probability density in the excited state wave function is the largest (see Fig. 4). These transitions populate vibrational v'' levels in the X (a) state with energy $E_{v''}^M$ approximately equal to $V_X(R_C^{in,out}(p_{1/2,3/2}))$ [$V_a(R_C^{in,out}(p_{1/2,3/2}))$], as indicated in Table I.

Stabilization at $R_C^{out}(p_{1/2})$ populates X and a levels with binding energy in the range of 2–15 cm^{-1}. Stabilization at $R_C^{out}(p_{3/2})$ concerns X (a) levels with larger binding energy of 75–110 cm^{-1} (50–90 cm^{-1}). Stabilization at the inner turning point of the adiabatic potential is possible only from the

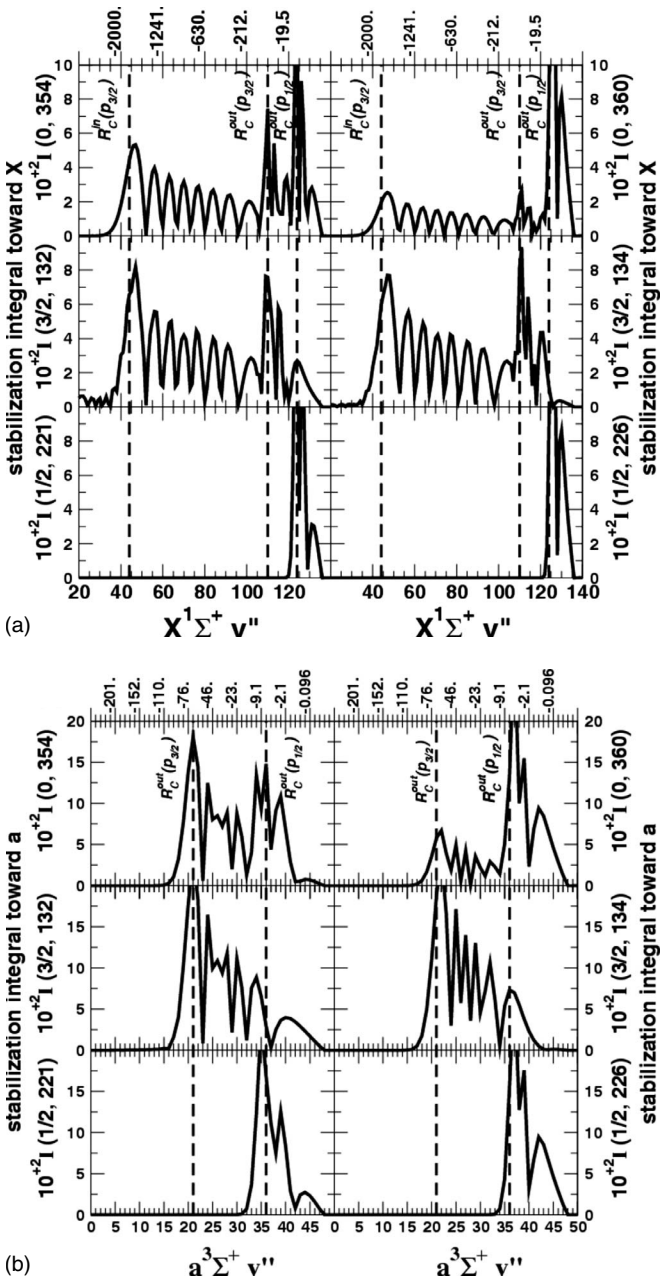

FIG. 6. Resonant coupling in the 0^+ electronic states: effects on radiative stabilization from the excited $|ev'\rangle$ level in the ^{85}RbCs molecule. The overlap integrals $I(e,v')$ (multiplied by 100) are drawn vs the vibrational quantum number v'' of the stabilized level (lower horizontal scale). For some v'' values, the energy $E_{v''}$ is indicated in cm^{-1} (upper horizontal scale). Different stable electronic states and excited levels are considered. Panel (a): $I(e,v')=|\langle ev'|Xv''\rangle|$; first line: overlap integrals $I(0,v')$ for the $|V'_+\rangle$ (left column) and $|V'_-\rangle$ (right column) levels; second line: overlap integrals $I(3/2,v_+)$ for the pure adiabatic levels $|P_{3/2}v_+\rangle$ with $v_+=132$ (left column) and $v_+=134$ (right column); third line: overlap integrals $I(1/2,v_-)$ for the pure adiabatic levels $|P_{1/2}v_-\rangle$ with $v_-=221$ (left column) and $v_-=226$ (right column). Panel (b): $I(e,v')=|\langle ev'|av''\rangle|$; same as above for the three lines (the v', v_+, and v_- values are indicated in the vertical scales). Notice that some maxima are truncated due to the plot range. Vertical transitions at the Condon points $R_C^{out}(p_{1/2,3/2})$ and $R_C^{in}(p_{3/2})$ are indicated by vertical dashed lines.

$V_{3/2}$ potential and toward the X state (see Fig. 1). It populates deep $|X\,^1\Sigma^+v''\rangle$ levels, bound by up to 2200 cm^{-1}.

The existence of transitions toward levels with binding energy larger than 15 cm^{-1} is due to nonadiabatic coupling between the $0^+(P_{1/2,3/2})$ channels. Such anomalous vibrational distributions, which could not be explained using FCFs calculated from pure adiabatic levels, were already ascribed to resonant coupling effects [37,70,71]. Comparing the overlap integrals for RS from either coupled $|0^+v'\rangle$ or adiabatic $|P_{1/2,3/2}v_\mp\rangle$ levels demonstrates that all $|0^+v'\rangle$ levels, even weakly coupled, possess properties arising from both types of adiabatic levels [see left and right columns in the first line of Figs. 6(a) and 6(b)]. There is in fact a global mixing between the levels of both adiabatic series.

In RbCs, the large binding energies $|E^M_{v''}|$ (see Table I) of the X and a levels populated by RS at $R_C^{out}(p_{1/2})$ $[R_C^{out}(p_{3/2})]$ are typical of a heteronuclear molecule. Indeed, due to the R^{-6} asymptotic form of the excited potential, stabilization from levels with a binding energy in the range of 10–100 cm^{-1} occurs at short range ($R\sim 15a_0$–$25a_0$), i.e., in a R range where the variation in the V_X and V_a potentials cannot be neglected. The $|E^M_{v''}|$ energies have to be compared to the corresponding ones, much smaller (respectively, $\sim 10^{-2}$ and 2–20 cm^{-1}) in the homonuclear $^{85}Rb_2$ molecule [37,70]. In the latter case, stabilization from an excited potential varying as R^{-3} occurs at large distance, $\sim 20a_0$–$25a_0$ and $60a_0$–$65a_0$, respectively, for $R_C^{out}(p_{3/2})$ and $R_C^{out}(p_{1/2})$, where the R dependence of the ground-state potential is almost negligible.

Concerning the FCFs (the square of the integrals I shown in Fig. 6) toward X levels, they are maximum at $R_C^{out}(p_{1/2})$, even for the strongly mixed $|V'_+\rangle$ level. For the latter level, the maximum FCF is only 2.6 times smaller than the maximum FCF for the $|V'_-\rangle$ level. For the $|V'_+\rangle$ level, the maximum values of the FCF at $R_C^{out}(p_{1/2})$, $R_C^{out}(p_{3/2})$, and $R_C^{in}(p_{3/2})$ are in the ratio 1:0.33:0.17. A large $0^+(P_{3/2})$ weight of the wave function results in large values of the FCF for transitions populating highly bound X levels ($|E_{v''}|>15$ cm^{-1}). The almost pure A character of the $|P_{3/2}\rangle$ adiabatic electronic state at $R_C^{in}(p_{3/2})$ (see Fig. 2) is at the origin of the relatively high value of the FCFs corresponding to transitions toward levels bound by ~ 2000 cm^{-1}. In contrast, for the $|V'_-\rangle$ level, the maximum values of the FCFs at the same three Condon points as above are in the ratio 1:0.016:0.014, pointing out the low probability of vertical transitions at $R_C^{in,out}(p_{3/2})$. Stabilization mainly populates high lying X levels.

Concerning RS toward a levels, at $R_C^{out}(p_{1/2})$, the FCFs from $|V'_-\rangle$ are larger by a factor of 4 than the FCFs from $|V'_+\rangle$. At $R_C^{out}(p_{3/2})$ they are smaller by a factor of 7.2. This reflects the large difference in the adiabatic channel mixing of the $|V'_\pm\rangle$ levels.

Stabilization toward the a state is much more favorable; the maximum FCFs are, in average, larger by a factor of approximately 4 than FCFs for stabilization toward the X state. For $|0^+v'\rangle$ levels close to the $Rb(5s)Cs(6p_{1/2})$ dissociation limit, the enhanced stabilization toward $a\,^3\Sigma^+$ results simultaneously from the predominant weight (60%) of the $|b\rangle$ diabatic state in the $|P_{1/2}\rangle$ adiabatic state at $R_C^{out}(p_{1/2})$ and from the nearly pure (90%) b character of the $|P_{3/2}\rangle$ adiabatic state at $R_C^{out}(p_{3/2})\sim R_{P_-}$ (see Fig. 2).

IV. FORMATION OF STABLE MOLECULES

The previous FCF calculations allow one to predict the vibrational distributions of stable X or a molecules formed after PA in the coupled 0^+ levels followed by RS. For an initially unpolarized gas (Rb, Cs) mixture, the four total spin states are equally distributed so that, for colliding pairs of atoms, triplet states are three times more probable than singlet states. This degeneracy ratio of 3:1 is not accounted for in this section.

A. Branching ratios for stabilization

For a $|0^+v'\rangle$ level, radiative stabilization toward X is the most favorable for vertical transitions occurring at the three Condon points $R_C^{out}(p_{1/2,3/2})$ and $R_C^{in}(p_{3/2})$; stabilization toward a state is the most favorable at the two Condon points $R_C^{out}(p_{1/2,3/2})$. Branching ratios for formation of stable molecules in bound levels $\bar{R}_j^i(v')$ characterizing these five different RS processes are defined from the partial sums of FCFs,

$$\bar{R}_j^i(v') = \sum_{v''=v_{min}^{i,j}(v')}^{v_{max}^{i,j}(v')} |\langle 0^+v'|iv''\rangle|^2, \tag{4}$$

with

$$i = X,a \text{ and } j = R_C^{in,out}(p_{1/2,3/2}),$$

where i denotes the stable electronic state and j the Condon point in the $V_{1/2,3/2}$ adiabatic potentials at the energy $E_{v'}$ of the $|0^+v'\rangle$ level. The limiting values $v_{min,max}^{i,j}(v')$ depend on the position of the Condon points j and therefore on the studied level v'. These limits have been deduced from the systematic study of the variation with v' and v'' of the FCFs $|\langle 0^+v'|iv''\rangle|^2$ for RS. Linear variations with v' have been chosen (see Ref. [44]). Only stable bound levels below the Rb(5s)Cs(6s) dissociation limit have been introduced in these branching ratios.

For a given electronic state i, the sum of the different branching ratios j,

$$\bar{R}^i(v') = \sum_j \bar{R}_j^i(v'), \tag{5}$$

gives the probability of formation of stable singlet or triplet molecules by RS from the $|0^+v'\rangle$ level.

The N stable X (or a) levels calculated with the mapped Fourier grid method define a complete set in the R space (N is the number of points in the spatial grid) [56]. Consequently, for a coupled level $|0^+v'\rangle$, the sum of FCFs over all the N singlet (or triplet) stable levels ($0 \leqslant v'' \leqslant N-1$), which includes bound molecules and pairs of free atoms, is equal to the weight of the singlet $|A\rangle$ (or triplet $|b\rangle$) component in the wave function of the $|0^+v'\rangle$ level. The probability of formation of free atom pairs in the stable X or a state (indicated in Table I) is simply deduced from the Hund case a representation of the wave function [see Eq. (2)] and from the probability $\bar{R}^i(v')$ of formation of bound molecules.

The numerical values for $\bar{R}_j^i(v')$ obtained for the $|V'_+\rangle$ and $|V'_-\rangle$ levels in ^{85}RbCs are reported in Table I. Concerning RS

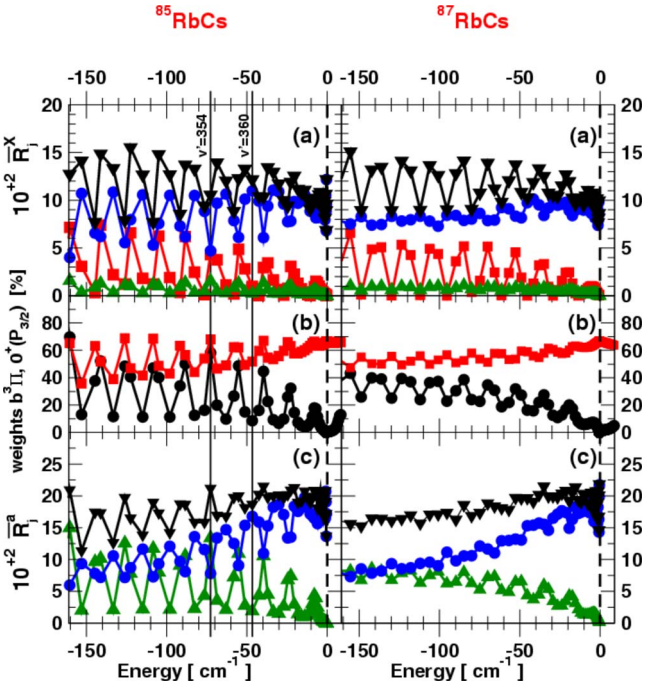

FIG. 7. (Color online) Radiative stabilization from the $|0^+v'\rangle$ coupled levels in the ^{85}RbCs (left column) and ^{87}RbCs (right column) molecules: branching ratios for stabilization toward the $i=X\,^1\Sigma^+$ [panels (a)] and the $i=a\,^3\Sigma^+$ [panels (c)] states at the Condon points $j=R_C^{in,out}(p_{1/2,3/2})$. The transition probability $\bar{R}_j^i(v')$ [Eq. (4)] multiplied by 100 is drawn as a function of the energy $E_{v'}$. The Rb(5s)Cs(6$p_{1/2}$) dissociation limit is indicated by the vertical dashed line. (a) $\bar{R}_j^X$ stabilization toward bound levels of the $X\,^1\Sigma^+$ state; total probability of forming bound stable X molecules $\bar{R}^X(v')$ [Eq. (5)] (black triangles down), probability of stabilization at $R_C^{out}(p_{1/2})$ (blue circles), at $R_C^{out}(p_{3/2})$ (green triangles up) and at $R_C^{in}(p_{3/2})$ (red squares). (b) Weight of the $0^+(P_{3/2})$ adiabatic channel [Eq. (A3)] (black circles) and weight of the $b\,^3\Pi$ diabatic channel [Eq. (2)] (red squares) in the $|0^+v'\rangle$ wave function. (c) $\bar{R}_j^a$ stabilization toward bound levels of the $a\,^3\Sigma^+$ electronic state; total probability of forming bound stable a molecules $\bar{R}^a(v')$ [Eq. (5)] (black triangles down), probability of stabilization at $R_C^{out}(p_{1/2})$ (blue circles) and at $R_C^{out}(p_{3/2})$ (green triangles up). The $|V'_+\rangle$ and the $|V'_-\rangle$ levels (Table I) are indicated by the vertical black continuous lines.

toward the X state, it is roughly equally probable at the outer Condon points of the $V_{3/2}$ and $V_{1/2}$ potentials for $|V'_+\rangle$; for $|V'_-\rangle$, it is ten times less probable at the outer Condon point of the $V_{3/2}$ potential. The stabilization at $R_C^{in}(p_{3/2})$ is significant for $|V'_+\rangle$. Concerning the stabilization toward the a state, the 0^+ level with a large $|V'_+\rangle$ ($|V'_-\rangle$) character stabilizes mainly at $R_C^{out}(p_{3/2})$ [$R_C^{out}(p_{1/2})$].

A strong isotopic effect is observed, in Fig. 7, in the variation in the branching ratios $\bar{R}_j^i(v')$ as a function of the energy $E_{v'}$ of the level. For 0^+ levels with $2 \leqslant E_{v'} \leqslant 150$ cm^{-1}, the Condon points $R_C^{in}(p_{3/2})$, $R_C^{out}(p_{3/2})$, and $R_C^{out}(p_{1/2})$ vary, respectively, in the range $6.76a_0$–$6.72a_0$, $17.56a_0$–$16.67a_0$, and $41.5a_0$–$21.1a_0$. Consequently, stable triplet a levels with binding energy increasing from 0.2 to 20 cm^{-1} (from 50 to 90 cm^{-1}) are populated by stabilization at $R_C^{out}(p_{1/2})$ [$R_C^{out}(p_{3/2})$]. Stabilization, respectively, at $R_C^{out}(p_{1/2})$,

$R_C^{out}(p_{3/2})$, and $R_C^{in}(p_{3/2})$ populates X levels with binding energies in the range of 0.3–20, 70–120, and 1600–2200 cm^{-1}.

The stabilization from the uppermost 0^+ levels with $|E_{v'}|<2$ cm^{-1} is very particular. The elongation of their outermost turning point $R_C^{out}(p_{1/2})$ increases rapidly with v' up to large distances of $\sim 130a_0$ (see Sec. III E). Stabilization from these levels mainly concerns the long-range part of the wave functions and efficiently populates the X and a levels lying very close to the dissociation limit.

Approximately 10%–15% of the molecules photoassociated in a $|0^+v'\rangle$ level are stabilized toward the X state and 15%–22% toward the a state. The remaining molecules yield pairs of hot atoms either in the X or in the a state. For ^{87}RbCs, the RS probability at $R_C^{out}(p_{1/2,3/2})$ varies smoothly with the energy of the $|0^+v'\rangle$ level, all wave functions presenting between these two outer turning points a similar adiabatic channel-mixing character (see Sec. III D). On the opposite, for ^{85}RbCs, the stabilization probability varies significantly, the maxima at $R_C^{out}(p_{3/2})$ corresponding to minima at $R_C^{out}(p_{1/2})$ and vice versa; these variations reproduce the variations in the $0^+(P_{3/2})$ character of the levels. Furthermore, the total stabilization probability is maximum for levels with the largest $0^+(P_{3/2})$ character.

For $|0^+v'\rangle$ levels with a large $0^+(P_{3/2})$ character, formation of tightly bound X levels, through radiative stabilization at $R_C^{in}(p_{3/2})$ can be as probable as the formation of weakly bound X levels at $R_C^{out}(p_{1/2})$. This property has already been noted in Ref. [50]. It arises from the strong adiabatic channel mixing and from the very similar energy variation at the inner walls of the ground V_X and excited V_A potentials, the latter potential being at small R nearly identical to the $V_{1/2}$ one.

For both isotopomers, the stabilization probability toward X levels at $R_C^{out}(p_{3/2})$, proportional to the weight of the $|P_{3/2}\rangle$ component in the wave function of the $|0^+v'\rangle$ level, is much smaller than the other two probabilities. For stabilization toward a levels, the two types of stabilization have similar probabilities for levels with a detuning larger than 100 cm^{-1}; close to the dissociation limit, stabilization at $R_C^{out}(p_{1/2})$ prevails. As discussed above, 0^+ levels very close to the Rb(5s)Cs(6$p_{1/2}$) dissociation limit stabilize only toward the two highest levels of the X and a electronic states.

B. Vibrational distribution of stable molecules

There are four different paths for formation of stable heteronuclear molecules through photoassociation in the $|0^+v'\rangle$ levels followed by radiative stabilization. The initial pair of atoms can be in a scattering level of the X or the a state and the molecules can be stabilized in bound vibrational levels of the X or the a state. For homonuclear molecules, because of the $g \leftrightarrow u$ selection rule for electric dipole transitions, there is no possible transfer of population between the $X\ ^1\Sigma_g^+$ and the $a\ ^3\Sigma_u^+$ states.

The efficiency of the four different paths (S or T) $\rightarrow$(S or T) can be evaluated from the quantities

$$R_{j\rightarrow i}(v') = |\langle jE_i = 75\ \mu\mathrm{K}|0^+v'\rangle|^2 \bar{R}^i(v'), \qquad (6)$$

where j and i denote the singlet X (S) or the triplet a (T) state. A single energy is considered in the pair of colliding atoms and the PA probability is given by the FCF only, the degeneracy factor of 1:3 being not introduced. The RS probability is evaluated from the branching ratio $\bar{R}^i(v')$ [Eq. (5)]. Since the scattering wave functions are energy normalized, $R_{j\rightarrow i}(v')$ is expressed in units of (energy)$^{-1}$, i.e., here, in $(E_h)^{-1}$. The variation of $R_{j\rightarrow i}(v')$ vs the energy $E_{v'}$ of the photoassociated level is presented in Fig. 8 for the ^{85}RbCs and ^{87}RbCs molecules. It is compared to the variation in the FCFs for photoassociation. Using the logarithmic scale allows one to show the energy dependence close to the Rb(5s)Cs(6$p_{1/2}$) dissociation limit, where the FCFs for PA present rapid oscillations with rapidly decreasing amplitude (see Sec. III E). The overall process of formation of stable molecules is larger for ^{87}RbCs than for ^{85}RbCs, especially for the $T\rightarrow T$ path and to a less extent for the $T\rightarrow S$ one.

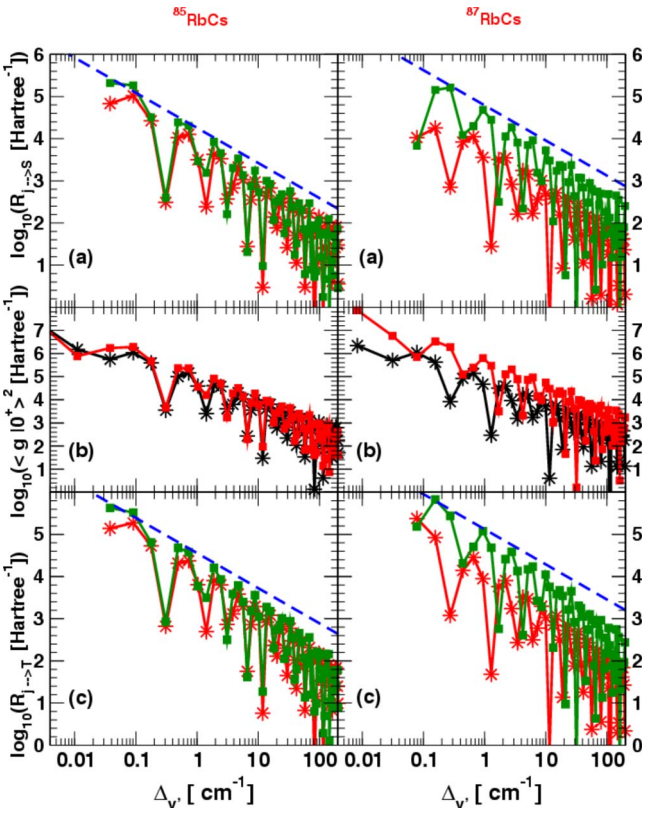

FIG. 8. (Color online) Formation of stable ^{85}RbCs (left column) and ^{87}RbCs (right column) molecules through photoassociation in a $|0^+v'\rangle$ level followed by radiative stabilization $R_{j\rightarrow i}(v')$ [Eq. (6)] as a function of the binding energy $\Delta_{v'}=|E_{v'}|$ of the level. Panel (a): formation of cold $X\ ^1\Sigma^+$ molecules from Rb and Cs atoms colliding either in the $X\ ^1\Sigma^+$ state ($S\rightarrow S$ path, red stars) or in the $a\ ^3\Sigma^+$ state ($T\rightarrow S$ path, green squares). A variation proportional to $\Delta_{v'}^{-5/6}$ is indicated by the blue dashed line. Panel (c): formation of cold $a\ ^3\Sigma^+$ molecules from Rb and Cs atoms colliding either in the $X\ ^1\Sigma^+$ state ($S\rightarrow T$ path, red stars) or in the $a\ ^3\Sigma^+$ state ($T\rightarrow T$ path, green squares). Panel (b): FCFs for photoassociation from a scattering level with energy $E_i=75$ μK either in the $X\ ^1\Sigma^+$ (black stars) or in the $a\ ^3\Sigma^+$ state (red squares).

The global variation in $R_{j\rightarrow i}(v')$ is determined by the energy variation in the FCFs for photoassociation, i.e., due to the reflection principle on the $V_{1/2}$ adiabatic potential, by the

nodal structure in the short-range part $R \leqslant R_N$ of the initial scattering wave functions (see Sec. III E). The nodal structure for the X and a scattering wave function is very similar for ^{85}RbCs (see Sec. III E), it differs for ^{87}RbCs due to a larger difference in the scattering length values in the X and a state (see Sec. II C).

For sufficiently small detuning, the asymptotic behaviors of the ground and excited potentials govern the variation in the FCFs as a function of $\Delta_{v'}$. Using the phase stationary approximation [73] and the asymptotic form of the ground-state wave function, scaling laws have been obtained (see Appendix B). In heteronuclear molecules, the decrease is $R_{j\to i}(v') \propto \Delta_{v'}^{-5/6}$, slower than in homonuclear molecules, where it varies as $\Delta_{v'}^{-7/6}$ [23]. These scaling laws, valid for $\Delta_{v'} < 10$ cm^{-1} [$R_C^{out}(p_{1/2} > R_N$], reproduce qualitatively the differences in the power-law dependences, respectively, $\Delta_{v'}^{-1}$ ($\Delta_{v'}^{-1.6}$) obtained from numerical values of FCF in ^{85}RbCs (^{85}Rb$_2$) calculated for $5 < \Delta_{v'} < 1000$ cm^{-1} [46].

The path $T \to T$ is the predominant one, the path $S \to S$ the smallest one. Among the two spin changing paths, the path $T \to S$ is generally a bit larger than the path $S \to T$, especially for the ^{87}RbCs molecule. The predominance of the $T \to T$ path is linked to the larger values for the FCFs for PA from the lowest triplet $a\ ^3\Sigma^+$ state and to the fact that the $|0^+ v'\rangle$ levels corresponding to an enhancement of the stabilization probability at $R_C^{out}(p_{3/2})$ have the largest $P_{3/2}$ and also b character (see Fig. 3). Furthermore, as discussed in Sec. III A, at the energy of the Rb($5s$)Cs($6p_{1/2}$) dissociation limit, both adiabatic channels $0^+(P_{1/2})$ and $0^+(P_{3/2})$ have a predominant $b\ ^3\Pi$ character. The predominance of this path is confirmed by the experiments of Kerman *et al.* [51], which show that $a\ ^3\Sigma^+$ levels with low binding energy are mostly populated through photoassociation in a laser-cooled mixture of ^{85}Rb and ^{133}Cs atoms; this is true even at a sufficiently low frequency of the photoassociating laser, where only the coupled 0^+ levels can by populated through PA.

V. CONCLUSION

In this paper, we have very carefully analyzed the sometimes subtle manifestations of the so-called resonant coupling in the formation of ultracold ^{85,87}RbCs molecules in the stable $X\ ^1\Sigma^+$ and $a\ ^3\Sigma^+$ electronic states through PA in the 0^+ coupled system followed by RS.

A mapped grid method was used to obtain the vibrational wave functions involved in the determination of the FCFs describing the PA and RS processes. Energies and wave functions in the coupled 0^+ system were calculated in Hund's case a description, introducing the Born-Oppenheimer diabatic potentials for the $A\ ^1\Sigma^+$ and $b\ ^3\Pi$ electronic states and their mutual electronic coupling through the R-dependent spin-orbit interaction.

The channel mixing effects are made obvious by introducing the adiabatic $0^+(P_{1/2})$ and $0^+(P_{3/2})$ electronic states and the pure adiabatic vibrational levels $|P_{1/2,3/2} v_{\mp}\rangle$ and by the analyzing the decomposition of the coupled $|0^+ v'\rangle$ levels on the Hund case c representation. A special attention is paid to the second crossing, which appears at $R_{x_2} \sim 21.5 a_0$, of the diabatic V_A and V_b^- potentials obtained when the diagonal spin-orbit interaction is added to the diabatic electronic potential V_b. The corresponding anticrossing between the adiabatic potentials $V_{1/2}$ and $V_{3/2}$ has a strongly avoided character and governs the properties of the levels involved in the PA process up to relatively large detuning (~ 500 cm^{-1}) below the Rb($5s$)Cs($6p_{1/2}$) dissociation limit. Calculation of the nonadiabatic couplings demonstrates their short-range character, mainly related to the presence of the strongly localized crossing at $R_{x_1} \sim 10 a_0$. Accounting in the model for a R-dependent spin-orbit interaction, which induces a decrease in the coupling strength at short distance ($R \sim R_{x_1}$), is necessary to reproduce the experimentally observed "global" mixing of the levels of the $0^+(P_{1/2})$ and $0^+(P_{3/2})$ adiabatic electronic states. The interference effects occurring in the calculation of the off-diagonal matrix elements of the nonadiabatic couplings explain the strong isotopic effect observed in the manifestation of the resonant coupling in the ^{85}RbCs and ^{87}RbCs molecules.

The coupled 0^+ system cannot be correctly described neither by pure Hund's case a levels nor by pure Hund's case c levels. Concerning the wave functions, there is a noticeable increase in the probability density at the four turning points $R_C^{in,out}(p_{1/2,3/2})$ of the two adiabatic $V_{1/2}$ and $V_{3/2}$ potentials. The relative importance of the maxima occurring at the outer turning points is indicative of the $0^+(P_{1/2})$ and $0^+(P_{3/2})$ adiabatic states mixing.

As photoassociation occurs mainly at large R, where the effects due to the crossing at R_{x_2} prevail, a description of the 0^+ coupled levels as pure adiabatic ones provides a correct estimation of the FCFs for PA. Their variation as a function of the binding energy of the photoassociated level can be related to the nodal structure in the initial scattering wave function by using the reflection principle on the $V_{1/2}$ potential. In heteronuclear molecules, due to the short-range character of the R^{-6} asymptotic form of the excited potentials, PA mainly involves the short range part of the initial wave function which has a relatively low amplitude. It explains the small values of the FCFs, except very close to the Rb($5s$)Cs($6p_{1/2}$) threshold (for $\Delta_{v'} < 2$ cm^{-1}), where the FCFs are larger and present rapid energy-dependent oscillations.

Concerning stabilization, the enhancement of the FCF for transitions $0^+ \to X$, due to the resonant coupling, is similar to the enhancement previously observed for Cs_2 and Rb_2 [37,45,70,71]. This effect is the largest for the $|0^+ v'\rangle$ levels with the largest $0^+(P_{3/2})$ character and induces the formation of deeply bound X and a molecules. For instance, the FCFs at $R_C^{out}(p_{3/2})$ of transitions $|0^+ v'\rangle \to |X\ ^1\Sigma^+ v''\rangle$ for coupled levels with $120 \geqslant \Delta_{v''} \geqslant 70$ cm^{-1} are larger by three orders of magnitude than the FCF's for RS from pure adiabatic levels $|0^+(P_{1/2}) v_-\rangle \to |X\ ^1\Sigma^+ v''\rangle$. Similar enhancement is observed for the RS at $R_C^{in}(p_{3/2})$ populating X levels with $2200 \geqslant \Delta_{v''} \geqslant 1600$ cm^{-1}.

Due to resonant coupling, levels reached by RS at $R_C^{out}(p_{3/2})$ have a much larger binding energy in RbCs (~ 100 cm^{-1}) than in Rb_2 (~ 5–20 cm^{-1}). The stable molecules formed in this way can be fruitfully used as starting point in an additional Raman process leading to RbCs mol-

ecules in the absolute ground level. As discussed for RbCs in Ref. [44] and as suggested for Rb_2 in Refs. [37,72], it is more efficient to start from these stable molecules than from that ones, with smaller binding energy, stabilized at $R_C^{out}(p_{1/2})$. The binding energy of the levels populated by RS at $R_C^{in}(p_{3/2})$, around 1500–2000 cm^{-1}, is very similar in RbCs and Rb_2.

For heteronuclear molecules, due to the absence of the $g-u$ symmetry, there is an additional possibility for producing stable molecules in the $a\ ^3\Sigma^+$ state, through stabilization from the 0^+ levels. The resonant coupling induces a strong enhancement of the $0^+ \rightarrow a$ radiative decay, efficiently populating a levels bound by 50–90 cm^{-1}. These levels could provide a starting point for spin-exchange Raman transitions, transferring the RbCs molecule toward low lying X vibrational levels.

Finally, analyzing and comparing the four different paths for the formation of stable RbCs molecules through PA of ultracold Rb and Cs atoms in the 0^+ state followed by RS, we have exhibited the predominance of the $T \rightarrow T$ path and the importance of isotopic effect, the overall process of formation of stable ^{87}RbCs molecules being one order of magnitude larger than the formation of stable ^{85}RbCs molecules.

This work is a first step in a more general study aiming to investigate the efficiency of the formation of stable heteronuclear dimers in the absolute ground state. In a forthcoming paper [44], we will present the formation of stable molecules in PA through intermediate 1 or 0^- levels below the $Rb(5s)Cs(6p_{1/2})$ dissociation limit followed by RS. Like in the 0^+ case studied here, we will show that this process essentially populates high lying $a\ ^3\Sigma^+$ levels. We will also propose several efficient spin-changing Raman processes through 0^+ and 1 intermediate levels. Using these Raman paths, in a next future, we will study the dynamics of the formation of ground-state molecules with tailored femtosecond pulses or trains of femtosecond pulses. The efficiency of these not yet investigated methods to form ground-state heteronuclear dimers will be compared to the efficiency of the already used STIRAP method.

ACKNOWLEDGMENTS

The authors thank Tom Bergeman for sending them his unpublished spin-orbit and diabatic potential results and Nadia Bouloufa, Christiane Koch, and Olivier Dulieu for fruitful discussions. This work is partially supported by grants from Région Ile-de-France. The authors are grateful to ECOS-NORTH for funding of the collaborative project C08P02 between the Instituto de Física, Universidad de Antioquia and the Laboratoire Aimé Cotton, Université Paris-Sud 11. B.L. thanks the Colombian agency for science, COLCIENCIAS, for supporting a stay at the Laboratoire Aimé Cotton, Orsay, where this work was initiated and for sponsoring a following collaborative visit. B.L. thanks the Relations Internationales de l'Université Paris-Sud 11 for their financial support. Laboratoire Aimé Cotton is unité propre UPR 3321 of CNRS associée à l'Université Paris-Sud 11, member of Fédération Lumière Matière (LUMAT, FR 2764) and of the Institut Francilien de Recherche sur les Atomes Froids (IFRAF).

APPENDIX A: ADIABATIZATION PROCEDURE

On the example of coupled 0^+ states, we recall in Appendix A 1 the general formulation of the transformation between diabatic and adiabatic representations as a rotation in a two-state model. The nonadiabatic couplings are analyzed in Appendix A 2.

1. Adiabatic electronic potentials

The adiabatic electronic states $0^+(P_{1/2,3/2})$ are obtained by diagonalizing, at any distance R, the diabatic potentials $V_i(R)$ ($i=A$ or $i=b$) and the spin-orbit coupling $W_{SO}^j(R)$ [Eq. (1)]. The R-dependent eigenvalues define the adiabatic potentials $V_{1/2}(R)$ and $V_{3/2}(R)$ converging toward the spin-orbit split dissociation limits $Rb(5s_{1/2})Cs(6p_{1/2,3/2})$. The diabatic (adiabatic) potentials present crossings (anticrossings) at R_{x_1} and R_{x_2}. The transformation from diabatic $\{|A\rangle, |b\rangle\}$ to adiabatic $\{|P_{1/2}\rangle, |P_{3/2}\rangle\}$ electronic basis is determined at each R by the rotation $\mathcal{R}(\theta)$ with angle $\theta(R)$,

$$|P_{1/2}\rangle = +\cos\theta(R)|b\rangle + \sin\theta(R)|A\rangle, \tag{A1a}$$

$$|P_{3/2}\rangle = -\sin\theta(R)|b\rangle + \cos\theta(R)|A\rangle. \tag{A1b}$$

[$\cos^2\theta$ gives at the distance R the weight of the diabatic triplet $|b\rangle$ (singlet $|A\rangle$) component in the $0^+(P_{1/2})$ [$0^+(P_{3/2})$] adiabatic channel.

The "pure adiabatic levels," in either the $0^+(P_{1/2})$ or the $0^+(P_{3/2})$ channel, are the vibrational levels calculated in a single potential $V_{1/2,3/2}$,

$$|P_{1/2,3/2}v_{\mp}\rangle = \frac{1}{R}\varphi_{1/2,3/2}^{v_{\mp}}(R)|P_{1/2,3/2}\rangle, \tag{A2}$$

The coupled wave functions $|0^+v'\rangle$, calculated in Hund's case a representation [see Eqs. (1) and (2)] using the diabatic $|A\rangle$ and $|b\rangle$ electronic wave functions, are decomposed on the basis of adiabatic electronic wave functions $|P_{1/2}\rangle$ and $|P_{3/2}\rangle$ by introducing the rotation $\mathcal{R}(\theta)$. In this representation, the two adiabatic channels are coupled by the nonadiabatic radial couplings (see Sec. III B). The wave functions for the $|0^+v'\rangle$ level can be written at a given R as

$$\begin{aligned}|0^+v'\rangle &= \Psi_{1/2}^{v'}(R)|P_{1/2}\rangle + \Psi_{3/2}^{v'}(R)|P_{3/2}\rangle \\ &= \frac{1}{R}[+\Psi_b^{v'}\cos\theta + \Psi_A^{v'}\sin\theta](R)|P_{1/2}\rangle \\ &\quad + \frac{1}{R}[-\Psi_b^{v'}\sin\theta + \Psi_A^{v'}\cos\theta](R)|P_{3/2}\rangle.\end{aligned} \tag{A3}$$

The radial functions $\Psi_{1/2,3/2}^{v'}$ are the adiabatic vibrational wave functions for the $|0^+v'\rangle$ level. The norm of each component gives quantitatively the weight of the adiabatic channels $0^+(P_{1/2})$ and $0^+(P_{3/2})$ in the coupled level $|0^+v'\rangle$.

2. Nonadiabatic couplings

The nonadiabatic radial couplings can be expressed in terms of $\theta(R)$ [65,74] as

$$\langle P_{1/2}v_-|\hat{T}_N|P_{3/2}v_+\rangle = -\frac{\hbar^2}{\mu}\left\langle \varphi_{1/2}^{v_-}\left|\frac{\partial\theta}{\partial R}\right|\frac{\partial\varphi_{3/2}^{v_+}}{\partial R}\right\rangle - \frac{\hbar^2}{2\mu}\left\langle \varphi_{1/2}^{v_-}\left|\frac{\partial^2\theta}{\partial R^2}\right|\varphi_{3/2}^{v_+}\right\rangle. \quad \text{(A4)}$$

They are predominant in the crossing regions R_{x_i}, where θ varies rapidly. Expressing θ in terms of the diabatic potentials and couplings defined in Eq. (1), neglecting the variation in the spin-orbit coupling around R_{x_i} and assuming linear variations $a_i(R-R_{x_i})$ for the vertical energy separation between the two diabatic potentials in the crossing regions, one obtains, near $R\sim R_{x_i}$, a Lorentzian variation for the first contribution in Eq. (A4),

$$\frac{\partial\theta}{\partial R} = \frac{a_i W_{\mathrm{SO}}^{off}(R_{x_i})}{4[W_{\mathrm{SO}}^{off}(R_{x_i})]^2 + a_i^2[R-R_{x_i}]^2}, \quad \text{(A5)}$$

with full width at half maximum $\delta R_{x_i} = 4W_{\mathrm{SO}}^{off}(R_{x_i})/a_i = [\partial\theta/\partial R|_{x_i}^{max}]^{-1}$, equal to the inverse of the maximum value of $\partial\theta/\partial R$, at $R\sim R_{x_i}$. This width depends on the description of the spin-orbit coupling.

APPENDIX B: SCALING LAW FOR THE PHOTOASSOCIATION RATE

For a cw laser tuned at resonance, the PA rate is proportional to the FCF $|\langle gE|ev'\rangle|^2$ (see Sec. II A). When PA occurs at sufficiently large distance, the asymptotic behavior of the potentials governs the process, resulting in scaling law with respect to the detuning $\Delta_{v'}$ of the photoassociated level in the excited potential $-C_n^e/R^n$. The vibrational wave function in the excited state has a sharp maximum at the Condon point $R_C(e,v')$, and in agreement with the image of a vertical transition where the vibrational motion is stopped, the excited wave function can be reduced to a δ function. In the stationary-phase approximation [73], the FCF is given by

$$|\langle gE|ev'\rangle|^2 \approx \frac{dE_{v'}^e}{dv'}\frac{1}{\mathcal{D}(R_C(e,v'))}|\Psi_E^g(R_C(e,v'))|^2. \quad \text{(B1)}$$

The level spacing in the excited state, $dE_{v'}^e/dv'$, is introduced to account for the normalization condition of bound states and $\mathcal{D}(R_C(e,v'))$ denotes the difference between the slopes of the two potential curves at the Condon point.

Using the long-range expression for Ψ_E^g, which is valid for $R_C(e,v')>R_N$, the following scaling law has been obtained for an homonuclear molecule (Eq. (45) in [23]):

$$|\langle gE|ev'\rangle|^2 \propto \mu E^{1/2}[C_3^e]^{2/3}\Delta_{v'}^{-7/6}. \quad \text{(B2)}$$

Similarly, for an heteronuclear molecule, where both potentials e and g decrease as R^{-6}, we obtain

$$|\langle gE|ev'\rangle|^2 \propto \mu E^{1/4}[C_6^e]^{4/3}\frac{1}{C_6^e - C_6^g}\Delta_{v'}^{-5/6}. \quad \text{(B3)}$$

Numerical values can be obtained for the $X\,^1\Sigma_g^+ \rightarrow 0_u^+(5p_{1/2})$ transition in $^{85}Rb_2$ [$X\,^1\Sigma^+ \rightarrow Rb(5s)Cs(6p)0^+(p_{1/2})$ in $^{85}RbCs$] using C_n coefficients given in [75] ([47]). We obtain, at a detuning $\Delta_{v'}=0.1$ cm^{-1}, the values of 1.81×10^{13}, (2.27×10^{12} a.u.) and, at a detuning $\Delta_{v'}=10$ cm^{-1}, the values of 8.35×10^{10}, (4.89×10^{10} a.u.). The atomic unit for a Franck-Condon factor is $[E_h]^{-1}$, where E_h is the atomic unit of energy. Very close to dissociation threshold, the Franck-Condon factor for the $^{85}Rb_2$ molecule is larger by a factor of $\sim$8.0 than the FCF for the $^{85}RbCs$ molecule. The decrease in FCF with the detuning ($\Delta_{v'}^{-7/6}$) is more rapid in Rb_2 than the variation in RbCs $\Delta_{v'}^{-5/6}$. Consequently, at a detuning 100 times larger the FCF for Rb_2 is larger by only a factor of $\sim$1.7.

[1] J. Doyle, B. Friedrich, R. V. Krems, and F. Masnou-Seeuws, Eur. Phys. J. D **31**, 149 (2004).
[2] L. D. Carr, D. DeMille, R. V. Krems, and J. Ye, New J. Phys. **11**, 055049 (2009).
[3] M. Aymar and O. Dulieu, J. Chem. Phys. **122**, 204302 (2005).
[4] M. G. Kozlov and L. N. Labzowsky, J. Phys. B **28**, 1933 (1995).
[5] D. DeMille, S. B. Cahn, D. Murphree, D. A. Rahmlow, and M. G. Kozlov, Phys. Rev. Lett. **100**, 023003 (2008).
[6] V. V. Flambaum and M. G. Kozlov, Phys. Rev. Lett. **99**, 150801 (2007).
[7] D. DeMille, S. Sainis, J. Sage, T. Bergeman, S. Kotochigova, and E. Tiesinga, Phys. Rev. Lett. **100**, 043202 (2008).
[8] T. Zelevinsky, S. Kotochigova, and J. Ye, Phys. Rev. Lett. **100**, 043201 (2008).
[9] K. Góral, K. Rzążewski, and T. Pfau, Phys. Rev. A **61**, 051601(R) (2000).
[10] D. DeMille, Phys. Rev. Lett. **88**, 067901 (2002).
[11] P. Rabl, D. DeMille, J. M. Doyle, M. D. Lukin, R. J. Schoelkopf, and P. Zoller, Phys. Rev. Lett. **97**, 033003 (2006); A. André, D. DeMille, J. M. Doyle, M. D. Lukin, S. E. Maxwell, P. Rabl, R. J. Schoelkopf, and P. Zoller, Nat. Phys. **2**, 636 (2006).
[12] S. F. Yelin, K. Kirby, and R. Côté, Phys. Rev. A **74**, 050301(R) (2006).
[13] R. V. Krems, Int. Rev. Phys. Chem. **24**, 99 (2005).
[14] E. R. Hudson, C. Ticknor, B. C. Sawyer, C. A. Taatjes, H. J. Lewandowski, J. R. Bochinski, J. L. Bohn, and J. Ye, Phys. Rev. A **73**, 063404 (2006).
[15] K. Góral, L. Santos, and M. Lewenstein, Phys. Rev. Lett. **88**, 170406 (2002).
[16] M. A. Baranov, M. S. Mar'enko, V. S. Rychkov, and G. V. Shlyapnikov, Phys. Rev. A **66**, 013606 (2002).
[17] B. Damski, L. Santos, E. Tiemann, M. Lewenstein, S. Kotochigova, P. Julienne, and P. Zoller, Phys. Rev. Lett. **90**, 110401 (2003).
[18] R. Barnett, D. Petrov, M. Lukin, and E. Demler, Phys. Rev. Lett. **96**, 190401 (2006).
[19] H. P. Büchler, E. Demler, M. Lukin, A. Micheli, N. Prokof'ev, G. Pupillo, and P. Zoller, Phys. Rev. Lett. **98**, 060404 (2007).

[20] J. M. Doyle, B. Friedrich, J. Kim, and D. Patterson, Phys. Rev. A **52**, R2515 (1995).
[21] H. L. Bethlem, G. Berden, and G. Meijer, Phys. Rev. Lett. **83**, 1558 (1999).
[22] C. A. Stan, M. W. Zwierlein, C. H. Schunck, S. M. F. Raupach, and W. Ketterle, Phys. Rev. Lett. **93**, 143001 (2004).
[23] F. Masnou-Seeuws and P. Pillet, Adv. At., Mol., Opt. Phys. **47**, 53 (2001).
[24] C. Ospelkaus, S. Ospelkaus, L. Humbert, P. Ernst, K. Sengstock, and K. Bongs, Phys. Rev. Lett. **97**, 120402 (2006).
[25] J. J. Zirbel, K. K. Ni, S. Ospelkaus, T. L. Nicholson, M. L. Olsen, P. S. Julienne, C. E. Wieman, J. Ye, and D. S. Jin, Phys. Rev. A **78**, 013416 (2008).
[26] M. Viteau, A. Chotia, M. Allegrini, N. Bouloufa, O. Dulieu, D. Comparat, and P. Pillet, Science **321**, 232 (2008).
[27] M. Viteau, A. Chotia, M. Allegrini, N. Bouloufa, O. Dulieu, D. Comparat, and P. Pillet, Phys. Rev. A **79**, 021402(R) (2009).
[28] J. G. Danzl, E. Haller, M. Gustavsson, M. J. Mark, R. Hart, N. Bouloufa, O. Dulieu, H. Ritsch, and H. C. Nägerl, Science **321**, 1062 (2008).
[29] F. Lang, K. Winkler, C. Strauss, R. Grimm, and J. Hecker Denschlag, Phys. Rev. Lett. **101**, 133005 (2008).
[30] W. C. Stwalley, Eur. Phys. J. D **31**, 221 (2004).
[31] M. Tscherneck and N. P. Bigelow, Phys. Rev. A **75**, 055401 (2007).
[32] J. M. Sage, S. Sainis, T. Bergeman, and D. DeMille, Phys. Rev. Lett. **94**, 203001 (2005).
[33] K.-K. Ni, S. Ospelkaus, M. H. G. de Miranda, A. Pe'er, B. Neyenhuis, J. J. Zirbel, S. Kotochigova, P. S. Julienne, D. S. Jin, and J. Je, Science **322**, 231 (2008).
[34] J. Deiglmayr, A. Grochola, M. Repp, K. Mörtlbauer, C. Glück, J. Lange, O. Dulieu, R. Wester, and M. Weidemüller, Phys. Rev. Lett. **101**, 133004 (2008).
[35] J. Deiglmayr, P. Pellegrini, A. Grochola, M. Repp, R. Côté, O. Dulieu, R. Wester, and M. Weidemüller, New J. Phys. **11**, 055034 (2009).
[36] O. Dulieu and F. Masnou-Seeuws, J. Opt. Soc. Am. B **20**, 1083 (2003).
[37] H. K. Pechkis, D. Wang, Y. Huang, E. E. Eyler, P. L. Gould, W. C. Stwalley, and C. P. Koch, Phys. Rev. A **76**, 022504 (2007).
[38] E. Luc-Koenig, R. Kosloff, F. Masnou-Seeuws, and M. Vatasescu, Phys. Rev. A **70**, 033414 (2004).
[39] E. Luc-Koenig, F. Masnou-Seeuws, and M. Vatasescu, Eur. Phys. J. D **31**, 239 (2004).
[40] E. Luc-Koenig and F. Masnou-Seeuws, in *Cold Molecules: Theory, Experiments and Applications*, edited by R. Krems, B. Friedrich, and W. Stwalley (CRC Press, Boca Raton, FL, 2009), p. 245.
[41] C. P. Koch, R. Kosloff, and F. Masnou-Seeuws, Phys. Rev. A **73**, 043409 (2006).
[42] J. Mur-Petit, E. Luc-Koenig, and F. Masnou-Seeuws, Phys. Rev. A **75**, 061404(R) (2007).
[43] C. P. Koch, E. Luc-Koenig, and F. Masnou-Seeuws, Phys. Rev. A **73**, 033408 (2006).
[44] B. Londoño, J. E. Mahecha, E. Luc-Koenig, and A. Crubellier (unpublished).
[45] C. M. Dion, C. Drag, O. Dulieu, B. Laburthe Tolra, F. Masnou-Seeuws, and P. Pillet, Phys. Rev. Lett. **86**, 2253 (2001).
[46] S. Ghosal, R. J. Doyle, C. P. Koch, and J. M. Hutson, New J. Phys. **11**, 055011 (2009).
[47] M. Marinescu and H. R. Sadeghpour, Phys. Rev. A **59**, 390 (1999).
[48] J. L. Roberts, J. P. Burke, Jr., N. R. Claussen, S. L. Cornish, E. A. Donley, and C. E. Wieman, Phys. Rev. A **64**, 024702 (2001).
[49] S. Azizi, M. Aymar, and O. Dulieu, Eur. Phys. J. D **31**, 195 (2004).
[50] A. J. Kerman, J. M. Sage, S. Sainis, T. Bergeman, and D. DeMille, Phys. Rev. Lett. **92**, 033004 (2004).
[51] A. J. Kerman, J. M. Sage, S. Sainis, T. Bergeman, and D. DeMille, Phys. Rev. Lett. **92**, 153001 (2004).
[52] M. Pichler, W. C. Stwalley, and O. Dulieu, J. Phys. B **39**, S981 (2006).
[53] C. Amiot, O. Dulieu, and J. Vergès, Phys. Rev. Lett. **83**, 2316 (1999).
[54] V. Kokoouline, O. Dulieu, and F. Masnou-Seeuws, Phys. Rev. A **62**, 022504 (2000).
[55] K. Willner, O. Dulieu, and F. Masnou-Seeuws, J. Chem. Phys. **120**, 548 (2004).
[56] V. Kokoouline, O. Dulieu, and R. Kosloff, J. Chem. Phys. **110**, 9865 (1999).
[57] S. Kallush and R. Kosloff, Chem. Phys. Lett. **433**, 221 (2006).
[58] A. R. Allouche, M. Korek, K. Fakherddin, A. Chaalan, M. Dagher, F. Taher, and M. Aubert-Frécon, J. Phys. B **33**, 2307 (2000).
[59] M. J. Jamieson, H. Sarbazi-Azad, H. Ouerdane, G.-H. Jeung, Y. S. Lee, and W. C. Lee, J. Phys. B **36**, 1085 (2003).
[60] E. Tiesinga, M. Anderlini, and E. Arimondo, Phys. Rev. A **75**, 022707 (2007).
[61] T. Bergeman (private communication).
[62] T. Bergeman, C. E. Fellows, R. F. Gutterres, and C. Amiot, Phys. Rev. A **67**, 050501(R) (2003).
[63] T. Bergeman, A. J. Kerman, J. M. Sage, S. Sainis, and D. DeMille, Eur. Phys. J. D **31**, 179 (2004).
[64] H. Fahs, A. R. Allouche, M. Korek, and M. Aubert-Frécon, J. Phys. B **35**, 1501 (2002).
[65] O. Dulieu and P. S. Julienne, J. Chem. Phys. **103**, 60 (1995).
[66] M. J. Seaton, Rep. Prog. Phys. **46**, 167 (1983).
[67] V. N. Ostrovsky, V. Kokoouline, E. Luc-Koenig, and F. Masnou-Seeuws, J. Phys. B **34**, L27 (2001).
[68] H. Jelassi, B. Viaris de Lesegno, and L. Pruvost, Phys. Rev. A **73**, 032501 (2006); **74**, 012510 (2006).
[69] O. Dulieu, P. Julienne, and J. Weiner, Phys. Rev. A **49**, 607 (1994).
[70] Y. Huang, J. Qi, H. K. Pechkis, D. Wang, E. E. Eyler, P. L. Gould, and W. C. Stwalley, J. Phys. B **39**, S857 (2006).
[71] A. Fioretti, O. Dulieu, and C. Gabbanini, J. Phys. B **40**, 3283 (2007).
[72] C. P. Koch, J. P. Palao, R. Kosloff, and F. Masnou-Seeuws, Phys. Rev. A **70**, 013402 (2004).
[73] H. Wang and W. Stwalley, J. Chem. Phys. **108**, 5767 (1998).
[74] H. Lefebvre-Brion and R. W. Field, *Perturbations in the Spectra of Diatomic Molecules* (Academic Press, London, 1986).
[75] T. Bergeman, J. Qi, D. Wang, Y. Huang, H. K. Pechkis, E. E. Eyler, P. L. Gould, W. C. Stwalley, R. A. Cline, J. D. Miller, and D. J. Heinzen, J. Phys. B **39**, S813 (2006).